



Originally published as:

Taran, M. N., Koch-Müller, M., Wirth, R., Abs-Wurmbach, I., Rhede, D., Greshake, A. (2009): Spectroscopic studies of synthetic and natural ringwoodite, γ -(Mg, Fe) $_2$ SiO $_4$. - Physics and Chemistry of Minerals, 36, 4, 217-232

DOI: 10.1007/s00269-008-0271-1

Spectroscopic studies of synthetic and natural ringwoodite,



Michail N. Taran¹, Monika Koch-Müller², Richard Wirth², Irmgard Abs-Wurmbach³, Dieter Rhede², Ansgar Greshake⁴

¹Institute of Geochemistry, Mineralogy and Ore Formation, National Academy of Science of Ukraine, Palladin Ave., 34, 03680 Kyiv-142, Ukraine,

E-mail: taran@igmr.relc.com

²GeoForschungsZentrum, Sektion 4.1, Telegrafenberg, 14473 Potsdam, Germany,

E-mail: mkoch@gfz-potsdam.de

³Institute of Applied Geosciences, Technical University Berlin, Ernst Reuter-Platz 1, D-10587

Berlin, Germany, E-mail: irmgard.abs-wurmbach@tu-berlin.de; irmgardAbs-wurmbach@alice-dsl.net (priv)

⁴Humboldt-Universität zu Berlin, Museum für Naturkunde, D-10099 Berlin, Germany,

E-mail: ansgar.greshake@museum.hu-berlin.de

Abstract

Synthetic ringwoodite $\gamma\text{-(Mg}_{1-x}\text{Fe}_x)_2\text{SiO}_4$ of $0.4 \leq x \leq 1.0$ compositions and variously colored micro-grains of natural ringwoodite in shock metamorphism veins of thin sections of two S6-type chondrites were studied by means of microprobe analysis, TEM and optical absorption spectroscopy. Three synthetic samples were studied in addition with Mössbauer spectroscopy. The Mössbauer spectra consist of two doublets caused by ${}^{\text{VI}}\text{Fe}^{2+}$ and ${}^{\text{VI}}\text{Fe}^{3+}$, with IS and QS parameters close to those established elsewhere (e.g. O'Neill et al. 1993). The $\text{Fe}^{3+}/\text{Fe}_{\text{total}}$ ratio evaluated by curve resolution of the spectra, ranges from 0.04 to 0.1. Optical absorption spectra of all synthetic samples studied are qualitatively very similar as they are directly related to the iron content. They differ mostly in the intensity of the observed absorption features. The spectra consist of a very strong high-energy absorption edge and a series of absorption bands of different width and intensity. The three strongest and broadest absorptions of them are attributed to splitting of electronic spin-allowed ${}^5T_{2g} \rightarrow {}^5E_g$ transitions of ${}^{\text{VI}}\text{Fe}^{2+}$ and intervalence charge-transfer (IVCT) transition between ferrous and ferric ions in adjacent octahedral sites of the ringwoodite structure. The spin-allowed bands at ca. 8000 and 11500 cm^{-1} weakly depend on temperature, whilst the $\text{Fe}^{2+}/\text{Fe}^{3+}$ IVCT band at $\sim 16400 \text{ cm}^{-1}$ displays very strong temperature dependence i.e., with increasing temperature it decreases and practically disappears at about 497 K, a behavior typical for bands of this type. With increasing pressure the absorption edge shifts to lower energies while the spin-allowed bands shift to higher energy and strongly decreases in intensity. The IVCT band also strongly weakens and vanishes at about 9 GPa. We assigned this effect to pressure-induced reduction of Fe^{3+} in ringwoodite.

By analogy with synthetic samples three broad bands in spectra of natural (meteoritic) blue ringwoodite are assigned to electronic spin-allowed transitions of ${}^{\text{VI}}\text{Fe}^{2+}$ (the bands at $\sim 8600 \text{ cm}^{-1}$ and $\sim 12700 \text{ cm}^{-1}$) and $\text{Fe}^{2+}/\text{Fe}^{3+}$ IVCT transition ($\sim 18100 \text{ cm}^{-1}$), respectively. Spectra of colorless ringwoodite of the same composition consist of a single broad band at ca. 12000 cm^{-1} . It is assumed that such ringwoodite grains are inverse $(\text{Fe}, \text{Mg})_2\text{SiO}_4$ -spinel and

that the single band is caused by the split spin-allowed ${}^5E \rightarrow {}^5T_2$ transition of ${}^{\text{IV}}\text{Fe}^{2+}$. Ringwoodite of intermediate color variations between dark-blue and colorless are assumed to be partly inversed ringwoodite. No glassy material between the grain boundaries in the natural colored ringwoodite aggregates was found in our samples and disprove the cause of the coloration to be due to light scattering effect (Lingemann and Stöffler 1998).

Key words: synthetic and natural ringwoodite, iron ions, optical spectroscopy at different temperatures and pressures, Mössbauer spectroscopy, TEM study

Introduction

Ringwoodite, γ -(Mg, Fe)₂SiO₄, a high-pressure spinel-type structure polymorph of olivine, is considered as the most abundant constituent of the lower part of the mantle transition zone. If so, its characteristics are an important clue for understanding geophysical properties of the Earth interior. That is why both natural (meteoritic) and synthetic ringwoodite are subject of numerous investigations since discovery of this mineral by Binns et al. (1969). However, among many publications devoted to ringwoodite one can find just a very few papers on optical absorption, FTIR and Mössbauer spectroscopic studies of synthetic ringwoodite (Mao and Bell 1972; O'Neill et al. 1993; Smyth et al. 2003; Jacobsen et al. 2004; McCammon et al. 2004; Keppler and Smyth 2005) and none at all on natural ones. At this juncture we present here results on optical absorption spectroscopy and on electron microprobe and TEM studies of a series of synthetic ringwoodite of (Mg_{1-x} Fe_x)₂SiO₄ compositions $0.4 \leq x \leq 1.0$ and variously colored meteoritic ringwoodite from two S6-type chondrites. In addition we present results on Mössbauer spectroscopy taken on three synthetic samples. The main purpose is to elucidate the state and structural positions of the predominant transition metal constituent of this mineral. The presence of iron may strongly influence crystal chemical, physical, thermodynamic and other properties of ringwoodite, as demonstrated in foregoing studies: starting from the pressure necessary for α to γ transformation (e.g. Syono et al. 1971, Mao and Bell 1972, Akimoto et al. 1976, Burns and Sung 1978) up to the influence on radiative thermal conductivity (Keppler and Smyth 2005), sound velocity and elastic properties (e.g. Sinogeikin et al. 1997) or seismic characteristics of the mantle (e.g. Sinogeikin et al. 2003).

Experimental methods

Sample characterization

Synthetic ringwoodite. $(\text{Mg, Fe})_2\text{SiO}_4$ -ringwoodite of different iron contents (Tab. 1) were synthesized in a 800 t multi-anvil press using 18/11 and 14/8 assemblies (octahedron edges length/truncated edge length). Details of the experimental procedures and set up are given in Deon et al. (2008). As starting material, we used either oxide mixtures (FeO , MgO and SiO_2) or synthetic fayalite, or a mixture of fayalite and oxides (MgO , SiO_2). To produce different oxygen fugacities, experiments were performed using a modified double capsule technique with water and a solid oxygen buffer placed at the bottom of the capsule and separated mechanically by a Pt disk from the starting material above. In all cases the buffer was active over the whole run duration. In each run ringwoodite was obtained as black non-transparent crystal fragments of irregular shapes together with pieces of a condensed powder of green and bluish-green color. The identifications of both, crystals and powder as ringwoodite were accomplished by X-ray diffraction and, in part, by Raman spectroscopy.

Natural ringwoodite. Natural (meteoritic) ringwoodite were available as thin sections (~ 12 μm thick) of the highly shocked (S6; Stöffler et al., 1991) L6-type ordinary chondrites NWA 1662 and NWA 463 from the collection of Museum für Naturkunde, Humboldt-Universität, Berlin. Ringwoodite occurs as transparent tiny grains of 10 to 100 μm in size predominantly within the opaque melt material of shock veins (cf. e.g. Binns et al. 1969). Color of ringwoodite grains varies from colorless to very dark-blue, nearly opaque. As a rule, homogeneously colored grains are rare. More frequently the color varies within one single crystal from colorless to blue and dark-blue. Sometimes a boundary between the colored parts of a single ringwoodite crystal is very distinct, but in most grains the color changes gradually displaying an irregular spotted distribution.

Several ringwoodite grains appropriate in size, coloration and quality for optical and FTIR spectroscopy were identified between crossed Nicols under a polarizing microscope. These visual identifications were then all proven by Raman spectroscopy. As an example, Raman spectra of blue and colorless zones of a double-colored ringwoodite grain in NWA 1662 thin section (sample #1, see below), selected for optical spectroscopic investigation, is shown in Fig. 1. In all cases studied

the natural ringwoodite grain material is found to be not a pure ringwoodite: in addition to strong ringwoodite lines, labeled in the Figure as R (cf. McMillan and Akaogi 1987), there is always some minor amount of wadsleyite, the β -modification of $(\text{Mg, Fe})_2\text{SiO}_4$, seen as weaker W-lines in the spectra. It is remarkable that the intensity ratio of the ringwoodite and wadsleyite lines is nearly constant in all crystals studied from the both meteorites, NWA 1662 and NWA 463.

Methods of investigations

Optical absorption spectra were measured in the range 370-1800 nm (ca. 27000-5555 cm^{-1}) with a single-beam microspectrophotometer constructed on basis of a SpectraPro-275 triple grating monochromator, highly modified mineralogical microscope MIN-8 and a PC. Ultrafluars 10 \times serve as objective and condenser. Two changeable highly stabilized quartz-halogen and Xenon lamps, both of 70 W, are used as light source. Two changeable photoelectric multiplying tubes and cooled PbS-cell are used as photodetectors. A mechanical high-stabilized 300 Hz-chopper and lock-in amplifier were applied to improve the signal/noise ratio. The spectra were scanned with steps $\Delta\lambda = 1$ nm, 2 nm and 5 nm in the range 270-450, 450-1000 and 1000-1800 nm, respectively. The diameter of the measuring spot was not larger than 100 μm .

The samples of synthetic ringwoodite for optical and NIR spectroscopic studies were prepared as thin sections of thickness, depending on iron content, from ca. 10 to 2 μm (Tab. 1). For this, visually homogenous grains of ringwoodite were selected under a binocular microscope. They were glued with epoxy on a supporting glass plate, polished with diamond powders and pastes upon one side, detached, turned over, fixed with epoxy again, grounded and polished on the opposite side until getting transparent thin sections, suitable for optical and NIR spectroscopic measurements. Still fixed on the supporting glasses with epoxy optical absorption and FTIR spectra of the thin sections were measured at ambient conditions in the range ~ 28000 -4000 cm^{-1} . The reference beam position was always taken on a supporting glass plate nearby the thin section measured.

To measure spectra at different temperatures and pressures the thin section of MA-62 and MA-68 ringwoodite (Tab. 1) were detached and cleaned from epoxy with acetone and ethanol.

The spectra at room and liquid nitrogen temperatures (~297 K and 77 K, respectively) were measured using a home-made miniature cryostat attached to the microspectrometer. The low temperature spectroscopic measurements in the UV-VIS-NIR, 27000-10000 cm^{-1} , were accomplished on a polished plate of ca. 10 μm thick prepared from ringwoodite MA-68. The sample was placed on a transparent supporting plate of synthetic high-quality single-crystal sapphire. Because the thermal conductivity of Al_2O_3 at low temperature is almost twice that of annealed pure copper (Volkov et al. 1981), it provides a very good thermal conductivity between the sample and sample holder of the cryostat. To maintain thermal contact, the sample was attached to the supporting plate and then to the cooled sample holder with vacuum grease. The cryostat was evacuated to pressure $\sim 10^{-3}$ torr. To avoid moisture condensation, the external surfaces of the windows were continuously blown with dry air.

A miniature electric furnace with an electronic control device was attached to the spectrophotometer. It provided temperature stability of ± 5 K and was used to register spectra at temperatures from 297 K to 497 K. The high temperature spectroscopic measurements in the UV-VIS-NIR, 27000-10000 cm^{-1} , were accomplished at 297, 397 and 497 K on a polished thin section of ca. 10 μm thickness prepared from ringwoodite MA-62.

High pressure spectroscopic measurements in the UV-VIS-NIR, 27000-10000 cm^{-1} , were performed on a polished, ca. 10 μm thick, thin section prepared from ringwoodite MA-62. To generate hydrostatic pressure up to ~ 12 GPa, the diamond anvils cell (DAC) technique was used as described elsewhere (*e.g.*, Langer 1990). Powder remission spectra of powdered ringwoodite were measured as described in Taran et al. (2004).

NIR spectra in the range 11000-4000 cm^{-1} were recorded at ambient conditions on a Bruker IFS 66v FTIR spectrometer. The spectrometer was equipped with a tungsten lamp light source, a quartz beam-splitter and a Hyperion microscope using Cassegrainian objectives and an

InSb detector. The spectra were taken with an aperture size of $50 \times 50 \mu\text{m}$ in case of synthetic ringwoodite and $10 \times 10 \mu\text{m}$ in case of natural ones. For each measurement the spectrum was averaged from 256 scans and the resolution was 2 cm^{-1} .

Optical absorption spectra were fitted with Gaussian components using Jandel Scientific software Peakfit 4.11. The main limitation of the procedure is the choice of a lineshape for the strong high-energy absorption edge overlapping the UV and part of the visible range in most of our spectra. This uncertainty frequently results in appreciable differences in energies, intensities, and widths of component Gaussian bands in spectra of different samples. On the basis of our experience with the set of spectroscopic functions available in Peakfit 4.11, the absorption edge is usually best fit by a sum of Gaussian and Lorentzian curves.

^{57}Fe -Mössbauer spectra were measured at room temperature using an originally 1.85 GBq ^{57}Co in Rh source. The principle construction of the equipment is similar to that described by Abs-Wurmbach and Amthauer (1988). Measurements were performed using a 1024 multichannel analyzer combined with a constant electrochemical drive system of triangular velocity wave form. Velocity scale is calibrated against metallic α -iron. IS-shifts from calibration spectra are used as gravity centre for the fitting procedure. Fits were performed assuming Lorentzian lines.

TEM investigations were carried out on a Tecnai F20-XTwin transmission electron microscope with a field emission gun as electron source. The TEM is equipped with a Gatan Tridiem™ filter, an EDAX X-ray analyzer with ultra thin window and a Fishione high angle annular dark field (HAADF) detector. TEM images were acquired as energy filtered images applying an energy window of 20 eV to the zero loss peak. EEL spectra were acquired with a dispersion of 0.1 eV/channel. The energy resolution of the filter was 0.9 eV at half width at full maximum of the zero loss peak. Spectra were acquired in diffraction mode with an acquisition time of 1 second.

The chemical compositions of the samples were determined by wavelength-dispersive X-ray analysis (WDS) techniques using a JEOL JXA-8500F (HYPERPROBE) electron microprobe at the GeoForschungsZentrum (GFZ) Potsdam. The analytical conditions included an acceleration voltage of 15 kV, a beam current of 20 nA, and a beam diameter of 1 μm . The following natural and synthetic standards were used: fayalite (Si, Fe), periclase (Mg), rhodonite (Mn), orthoclase (Al), wollastonite (Ca), rutile (Ti), NiO (Ni) and Cr_2O_3 (Cr). For all elements the peak counting times were 20 s; backgrounds were counted for 10 s. Matrix corrections were performed with the JEOL implementation by Paul Carpenter (version 3.50) of the CITZAF software (Armstrong 1995).

Results

Chemical compositions

Electron microprobe analyses of about ten spots on each synthetic ringwoodite sample were averaged and the formulae were calculated on the base of 4 oxygens (Table 1). The compositions range from the Fe-end-member to an intermediate composition in respect to Fe and Mg. The iron-end-member MA-75 and samples MA-102, MA-120 and MA-121 were synthesized under higher oxygen fugacity and should contain Fe^{3+} . We recalculated the EMP analyses to account for Fe^{3+} by increasing the Fe^{3+} content in expense of Fe^{2+} until the cation sums up to 3.0. However, as seen from the Table, only in the two latter and also in MA-75, which was grown without any buffer, recalculations of microprobe analyses result to some small concentrations of Fe^{3+} . As we added water to the system that was incorporated into the crystals the calculated Fe^{3+} content may be slightly overestimated due to possible vacancies to account for the water content.

By microprobe, the averaged crystal chemical formulae of two double-colored natural colorless-blue and blue-dark-blue ringwoodite grains (#1 and #2), selected for optical absorption and FTIR-spectroscopic studies, are very close to each other, $(\text{Mg}_{0.741}\text{Fe}_{0.251})_2\text{Si}_{1.002}\text{O}_4$ and

($\text{Mg}_{0.737}\text{Fe}_{0.258}$) $_2\text{Si}_{1.003}\text{O}_4$, respectively¹. Besides the three main oxides, MgO, FeO and SiO₂, in both samples minor amount of (in wt. %) MnO \cong 0.37, NiO \cong 0.04 and CaO \cong 0.02 were detected. TiO₂ and Cr₂O₃ were always below the detection limit. It is remarkable, that in a colorless-blue grain #1 the scanned profiles of three main components FeO, MgO and SiO₂ display essential homogeneity of the composition, independent on the color distribution (Fig. 2a), whereas in a blue-dark-blue grain #2, as seen from Fig. 2b, just a very weak increase of FeO-content at the expense of MgO takes place in the dark-blue zone. The same can also be seen from the composition maps (not shown): in the dark-blue zone the Fe-content is slightly higher than in the blue one, whilst the Mg-content distribution displays, as it should be, the opposite tendency. The Si-distribution is essentially homogeneous.

TEM study

High angle annular dark field images of the foil cut from the synthetic samples MA-75, MA-62 and MA-68 display a homogeneous non-grained structure without any additional phases aside ringwoodite.

Fig. 3a shows a HAADF image of a foil cut across a zoned (colorless-dark-blue) grain of natural ringwoodite from a thin section of the NWA 463 meteorite. As clearly seen, the material consists of micrograins (mosaic) of the size varying in the range of 500 nm up to a few microns. The curvature of the grain boundaries is convex and concave without 120° equilibrium angles at triple junctions. The curved grain boundaries indicate grain growth. Microstructure of the foil reveals no differences between the two zones, colorless and dark-blue.

High resolution images of the grain boundaries show that the lattice fringes from two adjacent grains are in contact thus indicating the absence of an amorphous phase along the grain boundaries (Fig. 3b). A comparison of the Fe L_{3,2} edges in natural ringwoodite (NWA 463) and synthetic ringwoodite (MA-68) reveals no differences between the spectra.

Mössbauer spectra

¹ The composition of each grain is nearly identical to the composition of the matrix olivine in respective thin sections. This observation is very common in S6-type chondrites (e.g. Sharp, DeCarli 2006).

The Mössbauer spectrum of synthetic ringwoodite MA-68 (Fig. 4) is very similar to that of MA-62 and MA-121. In all three samples Fe²⁺-absorption is the dominant one with about 96, 94 and 90 area% for MA-68, MA-62 and MA-121, respectively (Table 2). Total absorption in all cases is $\leq 3\%$. Linear absorption values of Fe³⁺ are only $\leq 0.1\%$. To avoid overlapping of these very faint lines of the doublet in one broad line, full width at half height (FWHM) of Fe³⁺ lines had to be fixed for sample MA-62 and MA-121. One fit for sample MA-68 with the highest total absorption was done without fixing the FWHM (Tab. 2). It should be mentioned that the background at the low-velocity side of sample MA-62 is a bit suspicious for a vanishing faint magnetic component.

Isomer shift (IS) and quadrupole splitting (QS) values are within errors (3σ) for all samples the same (Table 2). As expected from the synthesis conditions the Fe³⁺ content in sample MA-121 is higher than in MA-62 and MA-68. Despite the recalculations of the Fe³⁺ content of our electron microprobe data where we obtained Fe³⁺ in tetrahedral and octahedral coordinations, we interpret the IS and QS values of Fe³⁺ as indicative for octahedral coordination. They are in the same order of magnitude as those obtained by O'Neill et al. (1993). However we cannot rule out the possibility that small portions of Fe³⁺ are incorporated in tetrahedral coordination. As mentioned before, the recalculation gives only estimates as we do not consider the possibility of vacancies in the structures. Recalculating the crystal chemical formulas on the base of the Mössbauer and EMPA measurements for the three samples studied and neglecting the equilibrium of valence states results to the approximate composition of the run products: MA-68 (Fe³⁺/Fe_{tot} = 0.04) to (Mg_{0.50}Fe²⁺_{0.48}Fe³⁺_{0.02})₂Si_{0.99}O₄, MA-62 (Fe³⁺/Fe_{tot} = 0.06) to (Mg_{0.39}Fe²⁺_{0.57}Fe³⁺_{0.03})₂Si_{0.98}O₄ and MA-121 (Fe³⁺/Fe_{tot} = 0.1) to (Mg_{0.60}Fe²⁺_{0.37}Fe³⁺_{0.04})₂Si_{0.97}O₄. Fe³⁺/Fe_{tot} ratios are in the same range as those determined for γ -Fe₂SiO₄ and γ -(Mg, Fe)₂SiO₄ by O'Neill et al. (1993) and Keppler and Smyth (2005). Note, however, that only in MA-121 and MA-75 microprobe detects Fe³⁺ (cf. Table 1).

It should also be noted that McCammon et al. (2004) observed a relatively weak absorption with IS=0.61 mm/s and QS=0.85 mm/s and assigned it to quick electron transfer between Fe²⁺ and Fe³⁺. We cannot absolutely rule out the presence of such a doublet in our spectra but due to the low signal/noise ratio in this region we exclude it from the final results as it has no effect on the final Fe³⁺/Fe_{tot} ratios.

Optical absorption spectra

Synthetic ringwoodite. Absorption spectra of all synthetic ringwoodite studied qualitatively are rather similar. Representative spectra of four samples, MA-68, MA-120, MA-56 and MA-102 are shown in Fig. 5 together with results of the curve fitting for the first two. The spectra consist of a very strong high-energy absorption edge and a series of superimposed *a-* to *f-*bands of different intensities and widths. The characteristics of the component Gaussians, obtained by the curve fitting procedure for MA-68, are listed in Table 3. It is evident that the intensity of both the edge and the bands *a* to *f* strongly increase with iron content, but with the edge increasing much stronger than the bands. Thus, in the spectrum of MA-56 ringwoodite (*x*=0.780), taken on a thin section of ca. 5 μm (Fig. 5c), the bands *a* to *f* are seen just as poorly resolved envelope, whereas in MA-68 and MA-121 of significantly lower iron contents (*x*=0.5 and 0.4, respectively) these bands are much more distinct (Fig. 5, **a**, **b**). In the spectrum of the end-member ringwoodite MA-75 (not shown), measured on an extremely thin section of ca. 2 μm, these bands are seen just as a broad, practically unresolved shoulder superimposing a very strong edge cutting of a good deal of the visible range. In combination, the high-energy absorption edge and the superimposed *a-* to *f-*bands cause variously hued blue, bluish-green, grayish-green, olive etc., colors of the ringwoodite thin sections studied.

As seen from Fig. 5, there are noticeable differences in the relative intensities of the band *c* vs. bands *a* and *b* from sample to sample. In general, the band *c* is relatively higher in samples grown at higher oxygen fugacity and thus enriched with Fe³⁺ such as MA-102, MA-120 or MA-

121 (Table 1). The higher Fe³⁺-content is confirmed for MA-121 by Mössbauer spectroscopy (Result section, Table 2). Diffuse remission spectra (not shown), measured on powdered portions of each run product, closely remind the corresponding absorption spectra, e.g., showing a strong high-energy absorption edge with a weak shoulder caused by the *f*-band and a broad poorly resolved absorption envelope formed by overlapping bands *a*, *b* and *c*.

Spectra of two ringwoodite samples, MA-68 and MA-62, measured in the range 27000-10000 cm⁻¹ at four different temperatures are shown in Fig. 6, **a** and **b**, respectively: as the temperature decrease from 297 K to ~77 K, the *c*-band significantly grows, whereas the bands *a* and *b* remain almost unchanged (Fig. 6a). In addition the high-energy edge shifts with decreasing temperature to higher energies and noticeably changes in shape². The bands *d*, *e* and *f* become slightly narrower and, thus, better resolved but do not much change in intensity. During cooling the color of the thin section of MA-68 changes from bluish-green to blue. As the temperature increases from 297 K to 497 K the observed tendencies maintain: there is a significant increase in the intensity of the high-energy edge, which can be seen as a shift to lower energies with increasing temperature (Fig. 6b). Due to this effect the color of the ringwoodite thin section (~10 μm) clearly changes from grayish-green at room temperature to greenish-brown at 497 K. The temperature dependence of bands *a* and *b*, which are strongly superimposed by the growing edge, is very weak. They do not much change in both, energy and intensity, especially when compared with the *c*-band, which distinctly decreases with increasing temperature and practically disappears in the temperature range 397 to 497 K. Again, three weak bands, *d*, *e* and *f*, do not display any significant change. Within the uncertainty of the experiment their energies remain nearly constant, the bands become broader and, thus, less distinct with increasing temperature, such that at 497 K the *d*- and *e*-bands are almost not visible.

High-pressure spectra of MA-62 ringwoodite are shown in Fig. 7a. The intensity of the high-energy edge strongly increases with pressure as can be seen in its continuous shift to lower

² One has to take into account that at the low-temperature measurements the sample was attached to the transparent sapphire colder with a thin layer of vacuum grease. The latter may have contributed its own effects to the temperature dependence of, first of all, the absorption edge.

energies. Visually it is seen as change of the sample color from grayish-green to greenish-brown at pressure. In contrast to the edge, the *a*- and *b*-bands strongly decrease. Besides, they display distinct shifts to higher energies; the resulting absorption envelope becomes narrower and more symmetric in shape due to a stronger shift of the *a*-band compared to the band *b*: according to the curve fitting analysis (cf. Figs. 5**a**, **b** and 7**b**) the splitting between them changes from ~ 3630 cm^{-1} at ambient pressure (Tab. 3) to ~ 1290 cm^{-1} at 12.2 GPa.

The *c*-band continuously decreases and practically disappears at around 9 GPa without any noticeable change in energy. This is especially evident in view of the three weaker bands *f*, *d* and *e*, which also display practically no shift at pressure, but become more distinct in spite of strong overlapping with the increasing absorption edge. Note that the observed changes noticeably differ from what Keppler and Smyth (2005) saw in their ringwoodite spectra, where “neither the main crystal field band nor the charge transfer band show any significant broadening or change in intensity with pressure”. As seen from Fig. 7**b**, a satisfactory curve fit of the spectrum measured at 12.2 GPa does quite dispense with the *c*-band. Moreover, if the later had retained without any significant loss of intensity, it would have taken place just within the local minimum formed by the absorption edge and strongly weakened *b*- and *a*-bands (cf. also with Fig. 5, **a**, **b**) and, therefore, should have been well discernible in the original (unfitted) spectra measured at ca. 8.9 GPa or 12.2 GPa (Fig. 7**b**), but this is evidently not the case. It should be emphasized that the described pressure-induced changes are entirely reversible without any noticeable hysteresis.

Natural ringwoodite. Several differently colored crystals of meteoritic ringwoodite were studied by optical absorption spectroscopy. We distinguish two different types of spectra: one type represents spectra of blue ringwoodite independently on the intensity of the coloration and the second type represents spectra of colorless ringwoodite. Both types of spectra can be obtained as on homogeneously colored crystals as on differently colored zones of one crystal.

For example, absorption spectra measured on different zones of two double-zoned ringwoodite grains (colorless-blue and blue-dark-blue) from NWA 1662 (#1) and NWA 463 (#2, see Sample characterization section) meteorites are shown in Fig. 8, **a** and **b**, respectively, together with an unpolarized spectrum of matrix olivine (Fig. 8**a**). As seen from the Figure, spectra of the blue zones are rather similar in both grains and the spectrum of the dark-blue zone seems to differ from the latter only qualitatively, by a much higher intensity of the absorption features observed. The spectra consist of three distinct broad bands at energies ca. 9000 cm^{-1} , 12600 cm^{-1} and 18500 cm^{-1} , superimposed on the high energy absorption edge. By analogy with the synthetic ringwoodite (cf. Fig. 5), they are labeled as *a*-, *b*- and *c*-bands, respectively. Note that due to very high absorbance, frequently much higher than ~ 3.0 (Fig. 8**b**), the spectrum of the dark-blue ringwoodite in part is rather noisy. Despite of that, the three bands *a*, *b* and *c* at nearly the same energies as in the blue ringwoodite, can be perceived very clearly.

In the spectrum of colorless ringwoodite (Fig. 8**a**) there is only one broad band at ca. 12000 cm^{-1} , i.e. slightly lower than the *b*-band in spectra of blue ringwoodite (cf. the two spectra in Fig. 8**a**), superimposed on a relatively weak absorption edge.

Remarkably, the above mentioned absorption bands in the spectra of the colorless as well as in the spectra of the blue and, especially, of the dark-blue natural ringwoodite samples are several orders of magnitude higher than spin-allowed band of Fe^{2+} in matrix olivine of practically the same composition as ringwoodite. The spin-allowed band of the matrix olivine is perceptible in Fig. 8**a** only as a very weak feature around 9500 cm^{-1} upon the intense high-energy absorption edge causing the yellowish color of olivine grains.

Discussion

Synthetic ringwoodite. We assume that all spectroscopic features seen in the optical absorption spectra of our synthetic ringwoodite (Fig. 5) are caused by iron, as the intensities of all of them, the absorption edge and the bands *a* to *f*, strictly correlate with iron content. Note also that by TEM no other material than ringwoodite are observed in our synthetic samples.

Taking into account that by microprobe and Mössbauer spectroscopy from ~90 to 96 % of the total iron is Fe^{2+} (Tabs. 1, 2), it is reasonable to assume that the absorption edge in the optical spectra of the ringwoodite studied (Fig. 5) is mainly caused by UV-centered $\text{O}^{2-} \rightarrow \text{Fe}^{2+}$ charge-transfer bands which low-energy tail covers a part of the visible range. The observed lower energy shifts of the absorption edge with increasing temperature or pressure also support this assignment as it is rather typical for many iron-bearing oxygen-based minerals (e.g. Taran and Langer 2001; Mao 1976). From the fact that its intensity grows with iron content much stronger than the intensities of bands *a* to *f*, one may conclude that the UV $\text{O}^{2-} \rightarrow \text{Fe}^{2+}$ charge-transfer bands not only increase in intensity, but, very likely, significantly shift to lower energies with increasing iron concentration.

By widths and intensity ratio, the broad bands *a*, *b* and *c* in Fig. 5a closely resemble the three bands at $\sim 8680 \text{ cm}^{-1}$, $\sim 12270 \text{ cm}^{-1}$ and $\sim 17480 \text{ cm}^{-1}$, respectively, observed by Keppler and Smyth (2005) in the spectrum of their synthetic ringwoodite SZ0107 and one may assume that in the spectra of the samples studied here these bands are of similar nature, namely, related to the electronic spin-allowed ${}^5T_{2g} \rightarrow {}^5E_g$ transition of ${}^{\text{VI}}\text{Fe}^{2+}$ intensified by exchange interaction with neighboring Fe^{3+} (the bands *a* and *b*) and caused by $\text{Fe}^{2+}/\text{Fe}^{3+}$ IVCT (the band *c*)³. In favor of such an interpretation is the observation that the intensity ratio of the *c*-, *b*- and *a*-bands is obviously different in different samples (see Result section and, also, Fig. 5) thus evidencing that they undoubtedly belongs to, at least, two different centers. By curve fitting analysis the linear intensity ratio of the *a*-, *b*- and *c*-bands in our MA-68 ringwoodite is 1:4.3:2.8 (Tab. 3) which is close to that in Keppler and Smyth's sample, 1:4.5:2.6, although our sample has much higher iron content. In case of MA120 ringwoodite (Fig. 5b) the ratio is noticeably different, 1:4.1:3.5, at energies and half-widths of the bands close to those in MA-68 (cf. Fig. 5, a and b).

³ In our samples the energies of the three bands, *a*, *b* and *c*, are noticeably lower (Table 3) than in Keppler and Smyth's ringwoodite spectra. This difference may be explained by the concentration shift (see e.g. Burns 1993), as e.g., the iron content in MA-68 is nearly five times higher than in the sample of Keppler and Smyth (2005).

This clearly shows that the *c*-band's intensity is related to Fe³⁺-content and, taking into account its energy and width (Table 3), strongly supports its assignment to Fe²⁺/Fe³⁺ IVCT.

Keppler and Smyth (2005) assume that the abnormally high intensity of the spin-allowed bands *a* and *b* may be due to exchange interaction with neighboring Fe³⁺. So far such effect was established on a very restricted number of Fe²⁺, Fe³⁺-bearing silicates and its mechanism is not yet well understood. We agree that the bands *a* and *b* have an abnormally high intensity for ordinary spin-allowed bands. Indeed, calculated values of their molar absorptivity in our ringwoodite MA-68, 7.0 and 29.8 l·cm⁻¹·mol⁻¹, respectively, are more than twice lower than what Keppler and Smyth's estimated, 15.7 and 70.7 l·cm⁻¹·mol⁻¹. However, this is still too much for the ordinary spin-allowed ⁵T_{2g} → ⁵E_g bands of Fe²⁺ in octahedral coordination (cf. e.g. Burns 1993). Also, strong weakening of these bands with pressure and their weak temperature dependence are difficult to explain in view of the high regularity and centrosymmetric character of the octahedral site of the ringwoodite structure which accommodates ferrous ion. For instance, in case of strongly distorted acentric Fe²⁺(M2)O₆-octahedra in the orthopyroxene structure the intensities of the two spin-allowed *dd*-band of Fe²⁺(M2) originating from the split ⁵T_{2g} → ⁵E_g transition and averaged over three polarizations α, β and γ, are only around 4.6 and 16.2 l·cm⁻¹·mol⁻¹ (Goldman and Rossman 1978), i.e. almost twice lower than what we find in ringwoodite, 7.0 and 29.8 l·cm⁻¹·mol⁻¹ (see above). Yet, in orthopyroxene such bands undergo a considerable pressure-induced weakening caused by a decrease of the Fe²⁺(M2)O₆-octahedron distortion which results in a relaxation of the Laporte selection rule (Taran and Langer 2003). However, such a mechanism is hardly applicable to ringwoodite where Fe²⁺ is located in a nearly regular centrosymmetric octahedral site and one should not expect any significant pressure effect on intensity of the bands in question. On the other hand, we may assume that the absorption envelope, involving the *a*- and *b*-bands, becomes more symmetric with pressure (Fig. 7) due to decrease of the slight trigonal distortion of Fe²⁺O₆-octahedra and, thus, lowering of the

splitting between the two bands. The splitting may also be due to a dynamic Jahn-Teller effect on ${}^{\text{VI}}\text{Fe}^{2+}$. However, the influence of pressure on such Jahn-Teller centers is not yet known.

The weak temperature dependencies of the *a*- and *b*-bands in ringwoodite spectra (Fig. 6) are obviously at variance with temperature behavior of Fe^{2+} - Fe^{3+} pair bands in other minerals (Smith and Strens 1976; Smith 1978a, b; Mattson and Rossman 1987a; Taran et al. 1996; Taran and Rossman 2002). Besides, in all cases studied pressure induces strong intensification and leads the Fe^{2+} - Fe^{3+} pair bands shift to higher energies (Taran et al. 1996; Taran and Rossman 2002). In ringwoodite, as seen from Fig. 7, pressure does produce a similar shift of the bands *a* and *b* to higher energies, but its effect to their intensities is extraordinarily strong and just opposite to that of the Fe^{2+} - Fe^{3+} pair bands established in other minerals. Finally, if the bands *a* and *b* in ringwoodite was intensified by exchange effects with Fe^{3+} , we should have observed noticeable changes of their intensity with the degree of iron oxidation in the samples studied. But again this is not the case. Particularly, this is well seen when compare the spectra of MA-68 and MA-120 (Fig. 5, **a** and **b**) having close iron contents (0.5 and 0.4 a.p.f.u., respectively), but grown at different oxygen fugacity (Tab. 1): taking into account a similar thickness of these two samples, $\sim 10\ \mu\text{m}$, we may conclude that the intensities of the bands are not much different. Indeed, by the curve fitting analysis, the peak intensity of more prominent *b*-band is 0.68 and 0.62 in MA-68 and MA-120, respectively, just in accordance with their total iron contents.

Therefore, from the above reasoning one should conclude that aside from the abnormally high intensity, the *a*- and *b*-bands in ringwoodite spectra essentially differ from the Fe^{2+} - Fe^{3+} pair bands in other minerals. As yet we do not see any reasonable explanation for these bands intensification in ringwoodite spectra.

In difference to the *a*- and *b*-band, the in this study observed significant temperature dependence of the *c*-band, which distinctly diminishes and practically disappears at temperatures between 397 and 497 K, is consistent with its assignment by Keppler and Smyth (2005) to $\text{Fe}^{2+}/\text{Fe}^{3+}$ IVCT (e.g., Smith 1977; Smith and Strens 1976; Taran and Langer 1998).

Temperature dependence of IVCT bands is much stronger in case of symmetric $\text{Fe}^{2+}/\text{Fe}^{3+}$ IVCT's between ferrous and ferric ions accommodated in adjacent structurally equivalent positions than for asymmetric ones involving Fe^{2+} and Fe^{3+} in nonequivalent sites differing by size and symmetry (Taran and Langer 1998). In the ringwoodite structure Fe^{2+} and Fe^{3+} enter equivalent, nearly regular edge-sharing octahedra (e.g. Akimoto et al. 1976) and $\text{Fe}^{2+}\text{-Fe}^{3+}$ pairs, formed by the ions accommodated in the adjacent sites, ought to be highly symmetric. Therefore, the temperature effect on the $\text{Fe}^{2+}/\text{Fe}^{3+}$ IVCT band in ringwoodite spectra is expected to be relatively strong as is observed for the *c*-band.

As seen from Fig. 7, the *c*-band displays unusually strong pressure dependence continually decreasing and practically disappearing at around 9 GPa. To the best of our knowledge, so far no one observed such pressure induced effect to IVCT bands in other minerals or compounds (e.g. Abu-Eid 1976, Mao 1976, Taran and Langer 1998, Taran et al. 2007). It is also at variance with the observation of Keppler and Smyth (2005) on their ringwoodite SZ0107.

At the moment we can only assume, taking for granted that the *c*-band is really caused by $\text{Fe}^{2+}/\text{Fe}^{3+}$ IVCT, that its weakening and complete disappearance at pressure is caused by pressure-induced $\text{Fe}^{3+}\rightarrow\text{Fe}^{2+}$ reduction which leads to decrease of $\text{Fe}^{2+}\text{-Fe}^{3+}$ pair concentration in the structure. Such reaction does take place at high pressures in a great number of Fe^{3+} -bearing salts, complexes and compounds and, due to this phenomenon, the predominant form of iron in the lower mantle is assumed to be Fe^{2+} (Frank and Drickamer 1976). Note that our supposition on pressure-induced Fe^{3+} to Fe^{2+} reduction in ringwoodite is consistent with the observed reversible pressure behavior of the *c*-band (see Results): according to Frank and Drickamer (1976), Mössbauer spectra of ferric salts, complexes and compounds showing the pressure-induced reduction “upon release of pressure... returns substantially to the original ferric state”.

It is presumed that the pressure-induced reduction processes lead to generation of holes on the ligands which retain closely associated to the reduced iron sites. Materials exhibiting such iron reducing effect include halides, thiocyanates, phosphates, hydrates with H₂O as neighboring ligands, ferricyanides, metallorganic compounds and some other systems (Frank and Drickamer 1976). However, except, perhaps, for magnesioriebeckite (Burns et al. 1972), there is not any reliable experimental confirmation of such pressure-induced Fe³⁺→Fe²⁺ reduction in natural silicates and oxides. Therefore, as we believe, ringwoodite is the first mineral wherein such effect is observed by optical absorption spectroscopy⁴. Note that Frank and Drickamer (1976) also admit that “evidence for the reduction process may be obtained from optical measurements of the area under the charge-transfer peak”. They presume that in such case two opposite competing effects may take place, an increase in the transition moment with decreasing interatomic distances and a decrease in intensity due to the loss of ferric sites as they converted to ferrous ones. However, the first effect, i.e. the pressure-induced IVCT bands’ intensification, is not strong, at least, in oxygen-based minerals studied so far (Taran and Langer 1998, Taran et al. 2007). Therefore, the second effect, i.e. the decrease in intensity due to converting Fe³⁺ to Fe²⁺, prevails and we do observe a distinct reduction process in the high-pressure ringwoodite spectra as the decrease and disappearing of the Fe²⁺/Fe³⁺ IVCT band (Fig. 7).

The pressure, at which the *c*-band in ringwoodite completely disappears (~9 GPa), is rather low and it seems that in ringwoodite some structural or crystal chemical reasons facilitate the reduction process. As the composition and interatomic distances in the ringwoodite structure are out of something extraordinary (e.g. Akimoto et al. 1976), this may be the three-dimensional arrangement of edge-sharing Fe- and Mg-bearing octahedra in the spinel-type structure of γ-(Mg, Fe)₂SiO₄. Probably, it promotes formation and delocalization of the holes generated on O²⁻-ligands under the pressure-induced reduction process. Huggins (1976) considers that “pressure-

⁴ It is very unlikely that such effect can readily be detected by high-pressure Mössbauer spectroscopy as the Fe³⁺-content in synthetic ringwoodite is relatively low, less than ca. 10% of the total amount of iron (Tabs. 1, 2).

induced electron transfer” would be a more accurate description of such phenomenon than the “pressure-induced reduction”. Under such point of view the pressure-induced weakening and final disappearing of the $\text{Fe}^{2+}/\text{Fe}^{3+}$ IVCT band in ringwoodite may be regarded as a redistribution of the electron density between the Fe^{2+} - Fe^{3+} pairs involved in IVCT process and delocalization of the holes over the three-dimensional framework of the chains of octahedra running along the six face diagonals of the cubic cell. The strong intensification of the high-energy absorption edge (Fig. 7a) may, at least partly, be caused by holes generated during the reduction process.

The widths and intensities of the three other bands, *d*, *e* and *f*, are significantly smaller than those of *a*-, *b*- and *c*-bands (Table 3). They appear in spectra of all samples studied and are, most probably, related to spin-forbidden electronic transitions of $^{\text{VI}}\text{Fe}^{2+}$. According to the Tanabe-Sugano diagram for the electronic $3d^6$ -configuration (e.g. Burns 1993), these may be $^5T_{2g} \rightarrow ^3T_{1g}$, $\rightarrow ^3T_{2g}$ and $\rightarrow ^3E_g$ transition, respectively. They do not display any significant changes in energy and intensity except broadening with increasing temperature (Fig. 6). Also they do not much shift at pressure (Fig. 7). Such temperature and pressure behaviors are quite consistent with their assignment to spin-forbidden transitions of Fe^{2+} (cf. e.g. Abu-Eid 1976; Taran and Langer 2001; Taran and Langer 2003; Taran et al. 2007).

Finally, judging from the temperature and pressure effects on the spin-allowed and $\text{Fe}^{2+}/\text{Fe}^{3+}$ IVCT bands in ringwoodite, *a*, *b* and *c*, respectively, one may reasonably assume that at the mantle PT-conditions the radiative conductivity of ringwoodite may significantly differ from that at ambient temperature and pressure. This assumption is in agreement with the findings of Keppler and Smyth (2005).

Natural ringwoodite. In contrast to synthetic ringwoodite, whose spectra are strictly related to the iron content, the spectra of differently colored crystals or differently colored zones of single crystals of natural ringwoodite display striking differences despite of nearly identical chemical compositions (see Results section). Our results do not support the idea of Lingemann

and Stöfler (1998) that the natural (meteoritic) ringwoodite coloration is due to light scattering effect produced by the presence of a glassy material between the grain boundaries in colored ringwoodite aggregates. Although light scattering may, in principle, cause broad pseudo-absorption bands (e.g. Khomenko et al. 2002), our high-resolution TEM investigation of two foils cut off from a colorless to dark-blue ringwoodite grain in NWA 463 meteorite thin section across the both zones reveals no noticeable differences between the colorless and the dark-blue part. As seen from the Fig. 3a, the foil consists of numerous tiny microcrystals (mosaics) constituting the ringwoodite grain in the colorless and the dark-blue zone. All characteristics of the material in the two zones are found to be essentially identical. Electron diffraction showed that the grains are always a mixture of ringwoodite and some minor amount of wadsleyite. This result is in excellent agreement with our results on Raman spectroscopy (see the Sample characterization section). However, no glassy phase is detected in the foils studied: for instance, in Fig. 3b a distinct boundary between two micrograins is seen, but there is no sign of glassy material or some other phase in-between. Therefore, (and by analogy with synthetic ringwoodite (see below)) we suggest that the spectroscopic properties of both colored and colorless ringwoodite are due to the iron content, which, judging from the microprobe analyses (see Result section), is the only predominant transition metal constituent in natural ringwoodite studied.

Optical absorption spectra (Fig. 8) indicate that colorless and dark-blue ringwoodite can be regarded as two extreme states of this material, whereas all other color varieties, light-blue, blue etc., are intermediate combinations of these two. By analogy with synthetic samples, the three bands *a*, *b* and *c* in the spectra of natural samples may be regarded as being of a similar origin as the identical bands in spectra of synthetic ringwoodite (cf. Figs. 5 and 8). Thus, the bands *a* and *b* in Fig. 8 are to be attributed to the spin-allowed ${}^5T_{2g} \rightarrow {}^5E_g$ transition of ${}^{\text{VI}}\text{Fe}^{2+}$ split by the trigonal distortion or Jahn-Teller effect, whereas band *c* is caused by the $\text{Fe}^{2+}/\text{Fe}^{3+}$ IVCT.

In Fig. 9 the results of the curve-fitting procedure of the spectrum of blue ringwoodite (cf. Fig. 8a) are shown. As seen, quite similar to the synthetic ringwoodite (Fig. 5), this spectrum can be satisfactorily fitted by a high-energy edge, taken as a combination of Gaussian and a Lorentzian forms, and three *a*-, *b*- and *c*-Gaussians, well resolved and distinct in the original spectrum either. However, the energies and, especially, the widths of *a* to *c* bands are in this case significantly different from those in synthetic samples (cf. Tabs. 3, 4). Apparently, there is also a much better resolution of the bands in the spectra of the natural samples compared to the synthetic ones (cf. Figs. 5, 8).

The higher energies of the *a* to *c* bands in natural than in synthetic ringwoodite (cf. Tabs. 3, 4) may be due to the concentration shift caused by nearly twice lower iron content in these samples (see Results). However, a reason for the vivid differences in the widths, especially of the *a*- and *c*-bands, in spectra of natural and synthetic samples is not quite clear. As seen from Tables 3, 4, in synthetic samples the *c*-band is considerably broader than the *b*- and, especially *a*-band which can be explained by the different natures of the bands, Fe²⁺/Fe³⁺ IVCT and the spin-allowed *dd*-transition of ^{VI}Fe²⁺, respectively (e.g. Mattson and Rossman 1987b). Different to the synthetic ringwoodite, in natural ringwoodite the widths of all three bands, *a*, *b* and *c*, are rather commensurable (Tab. 4) which is at variance with the above mentioned observation by Mattson and Rossman (1987b). Currently the best explanation for these differences between synthetic and natural ringwoodite is the relatively low quality of the spectra measured on the extremely small grains or on differently colored zones of natural meteoritic ringwoodite and, thus, less reliable characteristics of the component bands obtained afterwards by the curve fitting procedure. Another reason might be a very short post-crystallization high-temperature annealing duration of the synthetic samples compared with meteoritic ones and thus a higher local residual straining in the structure causing broadening of the bands in the synthetic material.

The spectra of colorless natural ringwoodite, containing one single absorption band in the near infrared range at ca. 12000 cm⁻¹, is the most striking example of their complete difference

from what we see in spectra on the synthetic samples or on the blue natural ringwoodite of practically the same composition as the colorless ones. Of course, the tempting and simplest explanation would have been the intensification of *a*- and *b*-bands, as well as the appearance of *c*-band, due to higher oxidation state of iron in the blue and dark-blue varieties comparing with the colorless ones and, thus, appearance of exchange-coupled Fe^{2+} - Fe^{3+} pairs and pairs involved into $\text{Fe}^{2+}/\text{Fe}^{3+}$ IVCT process. However, taking into account the above deductions on synthetic ringwoodites and assuming that *a*-, *b*- and *c*-bands in natural ringwoodites are of the identical nature as in synthetic ones (see above), alternative models must be found. Note also that we did not produce colorless ringwoodite in our synthesis experiments at different oxygen fugacity. Again, we do not see any correlation between degree of oxidation and intensity of *a*- and *b*-bands in synthetic samples (see above), whereas in differently colored grains of natural ringwoodite of practically identical composition intensity of these bands varies about an order of magnitude (Fig. 8), but in difference to synthetic samples (Tab. 1), in natural ones the microprobe reveals no Fe^{3+} -concentration content at all (the Result section).

One explanation for the observed differences in the absorption spectra of natural colored and colorless varieties may be that iron occupies different structural positions in them, namely, that in colorless ringwoodite all iron as Fe^{2+} (and, likely, a part of magnesium also) enters the tetrahedral positions of the ringwoodite structure, whereas the silicon is distributed over the tetrahedral and octahedral sites, i.e., colorless ringwoodite is an inverse $(\text{Fe}, \text{Mg})_2\text{SiO}_4$ -spinel. Consequently, all intermediate color varieties between dark-blue and colorless ones are partially inverse ringwoodite. The possible inversion of the ringwoodite 2-4-spinel structure, i.e. the cation distribution of Mg, Fe^{2+} and Si over tetrahedral and octahedral sites, is yet poorly constrained (Hazen et al. 1993; O'Neill and Navrotsky 1983) because of similar X-ray scattering factors for Mg and Si. Ding et al. (1990) investigated synthetic Fe-end-member ringwoodite by X-ray powder diffraction and Rietveld refinement and found that the sample has a mixed normal-inverse spinel structure with ~40% of the silicon at the octahedral M site and ~20% of

the iron at the tetrahedral T sites. Also a first-principles computational study of the structural properties of ringwoodite shows that although it is unlikely that pure inverse ringwoodite is stable under the transition zone conditions (ca. 25 GPa and in excess of 1500 °C), there might be a considerable amount of inverse ringwoodite present (Kiefer et al. 1999). Impact events in space with cosmic velocities and large masses colliding are certainly able to generate much higher pressures and temperatures than those expected in the transition zone of Earth. Thus, in case of the S6 shock stage in ordinary chondrites, the pressure and temperature is evaluated as 75-90 GPa and 1500 °C, respectively (e.g., Stöffler et al., 1991; Taylor 2004). The presence of normal and inverse ringwoodite grains on a distance of a few hundreds or even a few tens of microns in meteoritic melt veins or even within one grain of less than a hundred micron of size with normal and inverse zones (zoned blue-colorless ringwoodite grains) evidences that the high-pressure olivine-ringwoodite phase transitions were likely caused by local pressure spikes which can induce shock pressures and temperatures varying, depending on details of local environment, by as much as an order of magnitude between grains or even within a single mineral grain (e.g. Sharp, DeCarli 2006).

The assumption that in colorless ringwoodite iron is in different structural position than in blue (dark blue) samples is consistent with our observation that in spectra of all colorless ringwoodite grains studied energy of the NIR band is considerably lower, down to 500 cm⁻¹, than that of the *b*-band in colored varieties (see also Fig. 8a). Obviously, this can not be due to the concentration shift as there is no difference in iron content between the colorless and colored varieties or the differently colored zones of single grains (Fig. 2). Besides, in spectra of colorless samples the NIR bands is always seen as a single band, not as *a*, *b*-doublet, as in the blue ones. We consider this as additional argumentation that these bands in question, in natural colorless and blue ringwoodite, are of different origin.

On the other hand, we must confess that the assumption that in colorless ringwoodite all iron is present as Fe²⁺ in tetrahedral coordination is, however, still rather a poor explanation for

the absorption band at 12000 cm^{-1} as spin-allowed ${}^5E \rightarrow {}^5T_2$ transition of ${}^{\text{IV}}\text{Fe}^{2+}$, especially taking into account the high symmetry of the site. In ${}^{\text{IV}}\text{Fe}^{2+}$ -bearing minerals such bands split because of the site distortion or by the dynamic Jahn-Teller effect and appear at much lower energies (Rossman and Taran 2001). Only if the coordination tetrahedron is strongly elongated as in beryl, osumilite or tuhualite (Taran and Rossman 2001) or degenerated up to the square-planar O^{2-} coordination as in gillespites or eudialite (Rossman and Taran 2001), the high energy band, derived from the electronic transitions from the ground to the split excited 5T_2 -state of ${}^{\text{IV}}\text{Fe}^{2+}$, appears at energies commensurable or even higher than the band at 12000 cm^{-1} in colorless ringwoodite. It is remarkable that the second, low energy band at around 5000 cm^{-1} , derived from the ${}^5E \rightarrow {}^5T_2$ transition of ${}^{\text{IV}}\text{Fe}^{2+}$, in beryl, osumilite or tuhualite is of a relatively low intensity, such that at low iron contents it is not even steadily detectable in the spectra.

In the normal ringwoodite structure the tetrahedral site is regular SiO_4 tetrahedron of T_d -point symmetry. By analogy with usual, non-silicate spinels, it seems certain that in the inverse ringwoodite the SiO_4 , MgO_4 and FeO_4 tetrahedra should also be regular, of the same symmetry, T_d (e.g. Baur 1972). On the other hand, it is not easy to predict the character of splitting of the electronic $3d$ -levels of Fe^{2+} of 5E -ground state undergone to Jahn-Teller effect in such unusual tetrahedral sites neighboring even more unusual SiO_6 -octahedra. It may be that our knowledge on electronic levels and optical absorption spectra of ${}^{\text{IV}}\text{Fe}^{2+}$ in other minerals is not strictly applicable to tetrahedral Fe^{2+} in the inverse ringwoodite structure. Therefore, we assume that although by energy the broad band at $\sim 12000\text{ cm}^{-1}$ in spectra of colorless ringwoodite does not quite correspond to what we expect for ${}^{\text{VI}}\text{Fe}^{2+}$, it may be caused by electronic spin-allowed ${}^5E \rightarrow {}^5T_2$ transition of ${}^{\text{IV}}\text{Fe}^{2+}$ in the structure of inversed ringwoodite. A low-energy band, if it does exist, may be too weak (see above) to be readily detected in spectra of extremely thin and small grains of meteoritic ringwoodite, or/and it may be shifted to low energies beyond the range studied.

Again, we must confess that the above interpretation of the spectra of synthetic and natural meteoritic ringwoodite leaves open several questions. First, it is the anomalously high intensity of the spin-allowed bands of Fe^{2+} in both synthetic and natural ringwoodite. Second, the unusually high energy of the absorption band caused by tetrahedral Fe^{2+} in colorless ringwoodite. Third, there is no explanation why the intensity of the spin-allowed bands of octahedral Fe^{2+} in the spectra of natural blue ringwoodite is much higher than the intensity of the spin-allowed bands of tetrahedral Fe^{2+} in spectra of colorless ringwoodite (cf. the spectra in Fig. 8), when, taking into consideration the selection rules for electronic dd -transitions (e.g. Burns 1993), it should be vice versa. Fourth, within the frame of this conception it is difficult to explain why we do not see any differences in the Fe $L_{3,2}$ edges in electron loss-energy spectra of dark-blue and colorless natural ringwoodite and, also, of synthetic ringwoodite. Taking into account that there is different distribution of Fe^{2+} among octahedral M- and tetrahedral T-sites one should expect differences of the Fe $L_{3,2}$ edges' structure in synthetic and natural samples (e.g. Egerton 1996), but this is not the case.

Conclusions

In synthetic ringwoodite iron enters octahedral sites of the structure predominantly as Fe^{2+} and, in minor amount, up to ca. 10 % of total content, in the form of Fe^{3+} . This is obvious from Mössbauer spectra which show the presence of only these two iron ion species. In optical absorption spectra, aside from the strong high-energy edge caused by $\text{O}^{2-} \rightarrow \text{Fe}^{2+}$ charge transfer UV transitions, iron ions cause a series of absorption bands. Three broad and most intense bands are caused by the electronic spin-allowed dd -transition of ${}^{\text{VI}}\text{Fe}^{2+}$ and the IVCT $\text{Fe}^{2+} + \text{Fe}^{3+} \rightarrow \text{Fe}^{3+} + \text{Fe}^{2+}$ transition between the ions in adjacent octahedral sites of the structure. The others are due to spin-forbidden transitions of Fe^{2+} . Temperature behaviors of the bands are in accordance with this interpretation. High-pressure absorption spectroscopy evidences a decrease of the IVCT band and its entire vanishing at around 9 GPa. This is interpreted as pressure-

induced reduction of Fe^{3+} in the ringwoodite structure, the first example observed by optical absorption spectroscopy in silicates.

By analogy with synthetic samples, three broad bands in spectra of natural (meteoritic) blue ringwoodite are assigned to electronic spin-allowed transitions of $^{\text{VI}}\text{Fe}^{2+}$ and $\text{Fe}^{2+}/\text{Fe}^{3+}$ IVCT transition. Spectra of colorless ringwoodite of the same composition consist of a single broad band in the near infrared. It is assumed that colorless ringwoodite grains are inverse $(\text{Fe}, \text{Mg})_2\text{SiO}_4$ -spinel and the above band is caused by the split spin-allowed transition of $^{\text{IV}}\text{Fe}^{2+}$. All intermediate color varieties between dark-blue and colorless ones are assumed to be partly inversed ringwoodite. No glassy material between the grains boundaries in colored ringwoodite aggregates which might cause coloration by the light scattering effect was found in our samples.

Acknowledgments

The German Science Foundation generously supported this work through grants 436UKR17/12/06 and KO1260/8-1. We would like to thank Dr. R. Thomas for the help with the Raman spectra and K. Paech for the TEM sample preparation. We are thankful to Hans Keppler and an anonymous reviewer for helpful comments which significantly improved the paper.

References

- Abs-Wurmbach I, Amthauer G (1988) Crystal Chemistry of iron in natural and synthetic braunites $\text{Mn}^{2+}(\text{Mn}^{3+}, \text{Fe}^{3+})_6\text{O}_8/\text{SiO}_4$. *Z Krist* 184: 13-30
- Abu-Eid RM (1976) Absorption spectra of transition metal-bearing minerals at high-pressure. In: Strens RGJ (ed) *The Physics and Chemistry of Minerals and Rocks*. Wiley, New York, 641-675
- Akimoto S, Matsui Y, Syono Y (1976) High-pressure crystal chemistry of orthosilicates and the formation of the mantle transition zone. In: Strens RGJ (ed) *The Physics and Chemistry of Minerals and Rocks*, New York, 327-363
- Armstrong JT (1995) CITZAF: A package of correction programs for the quantitative electron beam x-ray-analysis of thick polished materials, thin thin sections and particles. *Microbeam Analysis*, 4, 177-220
- Baur WH (1972) Computer-simulated crystal structures of observed and hypothetical Mg_2SiO_4 polymorphs of low and high density. *Am Mineral* 57: 709–731
- Binns RA, Davis RJ, Reed SJB (1969) Ringwoodite, natural $(\text{Mg}, \text{Fe})_2\text{SiO}_4$ spinel in the Tenham meteorite. *Nature*: 221: 943-944
- Burns RG (1993) *Mineralogical Applications of Crystal Field Theory*. (2nd ed) Cambridge University Press, Cambridge
- Burns RG, Sung C-M (1978) The effect of crystal field stabilization on the olivine→spinel transition in the system $\text{Mg}_2\text{SiO}_4 - \text{Fe}_2\text{SiO}_4$. *Phys Chem Minerals* 2: 349-364
- Burns RG, Tossell JA, Vaughan DJ (1972) Pressure-induced reduction of a ferric amphibole. *Nature* 240: 33-35
- Deon F, Koch-Müller M, Hövelmann J, Rhede D, Thomas S-M (2008) Coupled boron and hydrogen incorporation in coesite. *Europ. Journal Mineralogy* (in press)
- Ding J, Li D, Fu P (1990) X-Ray powder structural analysis of the spinel polymorph of Fe_2SiO_4 . *Powder Diffraction* 5: 221 – 222

- Egerton RF (1996) Electron loss-energy spectroscopy in electron microscope. Plenum, New York
- Jacobsen SD, Smyth JR, Spetzler H, Holl CM, Frost DJ (2004) Sound velocities and elastic constants of iron-bearing hydrous ringwoodite. *Phys Earth Planet Interiors* 143–144: 47–56
- Frank CW, Drickamer HG (1976) High pressure chemistry and physics of iron compounds. In: Strens RGJ (ed) *The Physics and Chemistry of Minerals and Rocks*. Wiley, New York, 509-544
- Hazen RM, Downs RT, Finger LW, Ko J (1993) Crystal chemistry of ferromagnesian silicate spinels: Evidence for Mg-Si disorder. *Am Mineral* 78: 1320–1323
- Huggins FE (1976) Mössbauer study of iron mineral under pressures up to 200 kilobars. In: Strens RGJ (ed) *The Physics and Chemistry of Minerals and Rocks*. Wiley, New York, 613-640
- Keppler H, Smyth RJ (2005) Optical and near infrared spectra of ringwoodite to 21.5 GPa: Implications for radiative heat transport in the mantle. *Am Mineral* 90: 1209-1212
- Khomenko VM, Langer K, Wirth R, Weyer B (2002) Mie scattering and charge transfer phenomena as causes of the UV edge in the absorption spectra of natural and synthetic almandine garnets. *Phys Chem Minerals* 29: 201-209
- Kiefer B, Stixrude L, Wentzcivitch R (1999) Normal and inverse ringwoodite at high pressures. *Am Mineral* 84: 288–293
- Langer K (1990) High pressure spectroscopy. In: Monttana A, Burrigato F (eds.) *Absorption Spectroscopy in Mineralogy*, Elsevier, 573-582
- Lingemann CM, Stöffler D (1998) New evidence for the colouration and formation ringwoodite in severely shocked chondrites. *Lunar Planet Sci* 29: #1308
- Mao HK, Bell PM (1972) Crystal-field stabilization of the olivine-spinel transition. *Carnegie Inst, Washington, Year Book* 71: 527-528

- Mao HK (1976) Charge-transfer processes at high pressure. In: Strens RGJ (ed) *The Physics and Chemistry of Minerals and Rocks*. Wiley, New York, 327-363
- Mattson SM, Rossman GR (1987a) Fe^{2+} - Fe^{3+} interactions in tourmaline. *Phys Chem Minerals* 14: 163-171
- Mattson SM, Rossman GR (1987b) Identifying characteristics of charge transfer transitions in minerals. *Phys Chem Minerals* 14: 94-99
- McCammon CA, Frost DJ, Smyth JR, Laustsen HMS, Kawamoto T, Ross NL, van Aken PA (2004) Oxidation state of iron in hydrous mantle phases: implications for subduction and mantle oxygen fugacity. *Phys Earth Planetary Interiors* 143-144: 157-169
- McMillan P, Akaogi M (1987) Raman spectra of β - Mg_2SiO_4 (modified spinel) and γ - Mg_2SiO_4 (spinel). *Am Mineral* 72: 361-364
- O'Neill HStC, McCommon CA, Canil D, Rubie DC, Ross CR, Seifert HF (1993) Mössbauer spectroscopy of mantle transition zone phases and determination of minimum Fe^{3+} content. *Am Mineral* 78: 456-460
- O'Neill HStC, Navrotsky A (1983) Simple spinels: crystallographic parameters, cation radii, lattice energies and cation distribution. *Am Mineral* 89: 181-194
- Rossman GR, Taran MN (2001) Spectroscopic standards for four- and fivefold-coordinated Fe^{2+} in oxygen-based minerals. *Am Miner* 86: 896-903
- Sharp TG, DeCarli PS (2006) Shock effects in meteorites. In: *Meteorites and the Early Solar System II*. Laurretta DS and McSween JrHY, eds, University of Arizona Press, Tucson, pp. 653-677
- Sinogeikin SV, Bass JD, Kavner A, Jeanloz R (1997) Elasticity of natural majorite and ringwoodite from the Catherwood meteorite. *Geophys Res Lett* 24: 3265-3268

- Sinogeikin SV, Bass JD, Katsura T (2003) Single-crystal elasticity of ringwoodite to high pressures and high temperatures: implications for 520 km seismic discontinuity. *Phys Earth Planet Inter* 136: 41-66
- Smith G (1977) Low-temperature optical studies of metal-metal charge-transfer transitions in various minerals. *Canad Mineral* 15: 500-507
- Smith G (1978a) A reassessment of the role of iron in the 5,000-30,000 cm^{-1} region of the electronic absorption spectra of tourmaline. *Phys Chem Minerals* 3:343-373
- Smith G (1978b) Evidence for absorption by exchange-coupled Fe^{2+} - Fe^{3+} pairs in the near infra-red spectra of minerals. *Phys Chem Minerals* 3:375-383
- Smith G, Strens RGJ (1976) Intervalence transfer absorption in some silicate, oxide and phosphate minerals. In: Strens RGJ (ed) *The Physics and Chemistry of Minerals and Rocks*. Wiley, New York, 583-612
- Smyth JR, Holl CM, Frost DJ, Jacobson SD, Langenhorst F, McCammon CA (2003) Structural systematics of hydrous ringwoodite and water in Earth's interior. *Am Miner* 88: 1402-1407
- Stöffler D, Keil, K, Scott ERD (1991) Shock metamorphism of ordinary chondrites. *Geochim Cosmochim Acta* 55: 3845-3867
- Syono Y, Tokonami M, Matsui Y (1971) Crystal field effect on the olivine-spinel transformation. *Phys Earth Planet Inter* 4: 347-352
- Taran MN, Dyar DM, Matsyuk SS (2007) Optical absorption study of natural garnets of almandine-skiagite composition showing intervalence $\text{Fe}^{2+} + \text{Fe}^{3+} \rightarrow \text{Fe}^{3+} + \text{Fe}^{2+}$ charge-transfer transition. *Am Miner* 92: 753-760
- Taran MN, Langer K (1998) Temperature and pressure dependence of intervalence charge transfer bands in spectra of some Fe- and Fe, Ti-bearing oxygen-based minerals. *N Jb Miner Abh* 172: 352-346

- Taran MN, Langer K (2001) Electronic absorption spectra of Fe^{2+} ions in oxygen-based rock-forming minerals at temperatures between 297 and 600 K. *Phys Chem Minerals* 28: 199-210
- Taran MN, Langer K (2003) Single-crystal high-pressure electronic absorption spectroscopic study of natural orthopyroxenes. *Eur J Mineral* 15: 689-695
- Taran MN, Langer K, Abs-Wurmbach I, Frost DJ, Platonov AN (2004) Local relaxation around $^{61}\text{Cr}^{3+}$ in synthetic pyrope-knorringite garnets, $^{81}\text{Mg}_3^{61}(\text{Al}_{1-x}\text{Cr}_x^{3+})_2^{41}\text{Si}_3\text{O}_{12}$, from electronic absorption spectra. *Phys Chem Minerals* 31: 650 – 657
- Taran MN, Langer K, Platonov AN (1996) Pressure- and temperature-effects on exchange-coupled-pair bands in electronic spectra of some oxygen-based iron-bearing minerals. *Phys Chem Mineral* 23: 230-236
- Taran MN, Rossman GR (2001) Optical spectroscopic study of tuhualite and a re-examination of the beryl, cordierite, and osumilite spectra. *Am Mineral* 86: 973–980
- Taran MN, Rossman GR (2002) High-temperature, high-pressure optical spectroscopic study of ferric-iron-bearing tourmaline. *Am Mineral* 87: 1148-1153
- Taylor GJ (2004) Asteroid Heating: A Shocking View. *Planetary Science Research Discoveries*.
<http://www.psr.d.hawaii.edu/April04/asteroidHeating.html>
- Volkov SYu, Grechushnikov BN, Sevastyanov BK, Tsvetkov VB (1981) A sapphire cold finger for getting intermediate temperatures. *Pribory i tehnika experimenta*, 2, 251-253 (in Russian)

Table 1. Characteristics of the synthetic ringwoodite samples studied.

| Sample No | Composition according to electron microprobe analysis | P(GPa)/ T (°C) | Oxygen buffer | Thin section thickness, μm | Thin section color |
|-----------|---|-------------------|---------------|---------------------------------------|--------------------|
| MA-121 | $(\text{Mg}_{0.61}\text{Fe}^{2+}_{0.38}\text{Fe}^{3+}_{0.02})_2(\text{Si}_{0.97}\text{Fe}^{3+}_{0.03})\text{O}_4$ | 14/1000 | MW | ~10 | blue |
| MA-120 | $(\text{Mg}_{0.60}\text{Fe}^{2+}_{0.39}\text{Fe}^{3+}_{0.02})_2(\text{Si}_{0.99}\text{Fe}^{3+}_{0.01})\text{O}_4$ | 14/1000 | NNO | ~10 | blue |
| MA-68 | $(\text{Mg}_{0.50}\text{Fe}_{0.50})_2\text{SiO}_4$ | 14/1000 | IW | ~10 | bluish-green |
| MA-62 | $(\text{Mg}_{0.39}\text{Fe}_{0.61})_2\text{SiO}_4$ | 14/1000 | IW | ~10 | grayish-green |
| MA-102 | $(\text{Mg}_{0.28}\text{Fe}_{0.72})_2\text{SiO}_4$ | 14/1000 | QFM | ~10 | bluish-green |
| MA-56 | $(\text{Mg}_{0.22}\text{Fe}_{0.78})_2\text{SiO}_4$ | 14/1200 | IW | ~5 | olive |
| MA-75 | $(\text{Mg}_{0.03}\text{Fe}^{2+}_{0.92}\text{Fe}^{3+}_{0.05})_2(\text{Si}_{0.95}\text{Fe}^{3+}_{0.05})\text{O}_4$ | 7/1100 | no | ~2 | olive |

Abbrev.: F Fayalite, I iron, M magnetite, N nickel, NO nickel oxide, Q quartz, W wüstite

Table 2. Fit-values of Mössbauer spectra of synthetic ringwoodite MA-68, MA-62 and MA-121

| Sample | Exp/calc | Fe ²⁺ | | | | Fe ³⁺ | | | |
|--------|----------|------------------|----------|------------|--------|------------------|----------|-------------|--------|
| | | IS, mm/s | QS, mm/s | FWHM, mm/s | Area % | IS, mm/s | QS, mm/s | FWHM, mm/s | Area % |
| MA-68 | 1.004 | 1.05 | 2.78 | 0.29 | 96.0 | 0.14(2) | 0.43(4) | 0.31(5) | 4.0 |
| MA-68 | 1.003 | 1.05 | 2.78 | 0.29 | 95.9 | 0.14(3) | 0.43(4) | 0.35 | 4.1 |
| MA-62 | 1.017 | 1.06 | 2.76 | 0.31 | 94.2 | 0.25(2) | 0.38(2) | 0.35 | 5.8 |
| MA-121 | 1.024 | 1.07 | 2.78 | 0.27 | 90.0 | 0.25(2) | 0.40(3) | 0.35 | 10.0 |

Calibrated against metallic α -iron. **Bold**: fixed values. Errors in 1σ : Fe²⁺-parameters less than one in the last digit; Fe³⁺ parameters are depending on the fixed values of FWHM.

Table 3. Results of curve fitting in the energy range 27,000-4,000 cm^{-1} of the spectrum of synthetic ringwoodite MA-68 at ambient conditions (cf. Fig. 5a). I_0 and I is intensity of the reference and sample beam, respectively. d is thickness of the sample in cm. FWHM is full band width at half maximum height.

| Band | Energy, cm^{-1} | Linear intensity, $\log(\frac{I_0}{I})$ | Linear absorption coefficient $\frac{1}{d}\log(\frac{I_0}{I})$, cm^{-1} | FWHM, cm^{-1} |
|----------|-----------------------------|--|---|---------------------------|
| <i>a</i> | 7900 | 0.159 | 159 | 2904 |
| <i>b</i> | 11530 | 0.677 | 677 | 4535 |
| <i>c</i> | 16384 | 0.442 | 442 | 5615 |
| <i>d</i> | 19142 | 0.036 | 36 | 1200 |
| <i>e</i> | 19854 | 0.002 | 2 | 538 |
| <i>f</i> | 21738 | 0.127 | 127 | 1819 |

Table 4. Results of curve fitting in the energy range 27,000-4,000 cm^{-1} of the spectrum of natural blue ringwoodite from the L6 chondrite NWA 1662 at ambient conditions (cf. Fig. 9). I_0 and I is intensity of the reference and sample beam, respectively. FWHM is full band width at half maximum height.

| Band | Energy, cm^{-1} | Linear intensity, $\log\left(\frac{I_0}{I}\right)$ | FWHM, cm^{-1} |
|----------|-----------------------------|---|---------------------------|
| <i>a</i> | 8600 | 0.236 | 3450 |
| <i>b</i> | 12680 | 0.626 | 4150 |
| <i>c</i> | 18100 | 0.388 | 4200 |

Figure captions

Fig. 1. Raman spectra of blue and colorless zones of a zoned grain (sample #1) of natural ringwoodite in the thin section of the L6 chondrite NWA 1662. R and W denote the lines related to ringwoodite and wadsleyite phase, respectively. The broad structured band at around 225 cm^{-1} is due to glassy melted phase produced by heating of the laser beam.

Fig. 2. Profiles of microprobe MgO, FeO and SiO₂ contents traced through differently colored zones of double-colored grain in the thin section of: **a**- NWA 1662 (sample #1) and **b**- NWA 463 (sample #2) L6 chondrites. The first point in **a** is taken very close to the boundary of the grain. Therefore, the data obtained in this point are, most likely, averaged between the ringwoodite grain and the black nontransparent material of the shock metamorphism vein. That why this point drops out of the profiles.

Fig. 3. **a**- HAADF image of a thin foil of natural zoned colorless-dark-blue ringwoodite cut over the both zones. No differences between colorless and dark-blue zones are seen. **b**- Image of a boundary between two micrograins of ringwoodite in the dark-blue zone. No evidence of glassy material within the boundary between the grains is seen.

Fig. 4. Mössbauer spectrum of synthetic ringwoodite MA-62 (see Tab. 1). Two quadrupole doublets, the major one with $IS \approx 1.06$ and $QS \approx 2.76$ mm/sec and the junior one with $IS \approx 0.25$ and $QS \approx 0.38$ mm/sec are caused by $^{VI}\text{Fe}^{2+}$ and $^{VI}\text{Fe}^{3+}$, respectively. The calculated integral intensity ratio of the two QD results to $\text{Fe}^{3+}/\text{Fe}_{\text{tot}} = 0.07$.

Fig. 5. Optical absorption spectra of thin sections of four synthetic ringwoodite of different composition, MA-68, MA-120, MA-56 and MA-102 (cf. Tab. 1). For MA-68 (**a**) and MA-120 (**b**) the result of the curve fitting procedure is also shown. Three broad and intense bands, *a*, *b* and *c*, and three weaker and much narrower bands *d*, *e* and *f*, distinct in the original spectrum, together with the intense high-energy edge, approximated by a sum of a Gaussian and Lorentzian, result to a satisfactory resolution of the spectra. In spectrum of partly oxidized

ringwoodite MA-102 (Fig. 5d) predomination of the *c*-band over bands *a* and *b* causes a broad asymmetric absorption envelope with a very smooth maximum at around 15000 cm⁻¹.

Fig. 6. Absorption spectra of MA-68 (a) and MA-62 ringwoodite (b) measured at different temperatures. Intensity of the *c*-band (denoted at the Figure as Fe²⁺/Fe³⁺ IVCT) displays rather strong temperature dependence different from that of the *b*-band, which practically does not change with temperature.

Fig. 7. a- Absorption spectrum of MA-62 ringwoodite (Tab. 1) measured at different pressures. For the sake of clarity the spectra are shifted along the vertical direction. b- The result of the curve fitting procedure of the spectrum measured at 121.9 kbars (ca. 12.2 GPa).

Fig. 8. Optical absorption spectra of differently colored zones in two crystals of natural ringwoodite: a-colorless-blue ringwoodite in the thin section of the L6 chondrite NWA 1662 (sample #1). For comparison spectrum of matrix olivine of nearly the same composition as differently colored ringwoodite is also shown; b- blue-dark-blue ringwoodite grain in the thin section of the L6 chondrite NWA 463 meteorite (sample #2).

Fig. 9. Result of the curve resolution of the spectrum of blue zone of zoned ringwoodite grain (sample #1) in the thin section of the L6 chondrite NWA 1662 (cf. Fig. 8a).

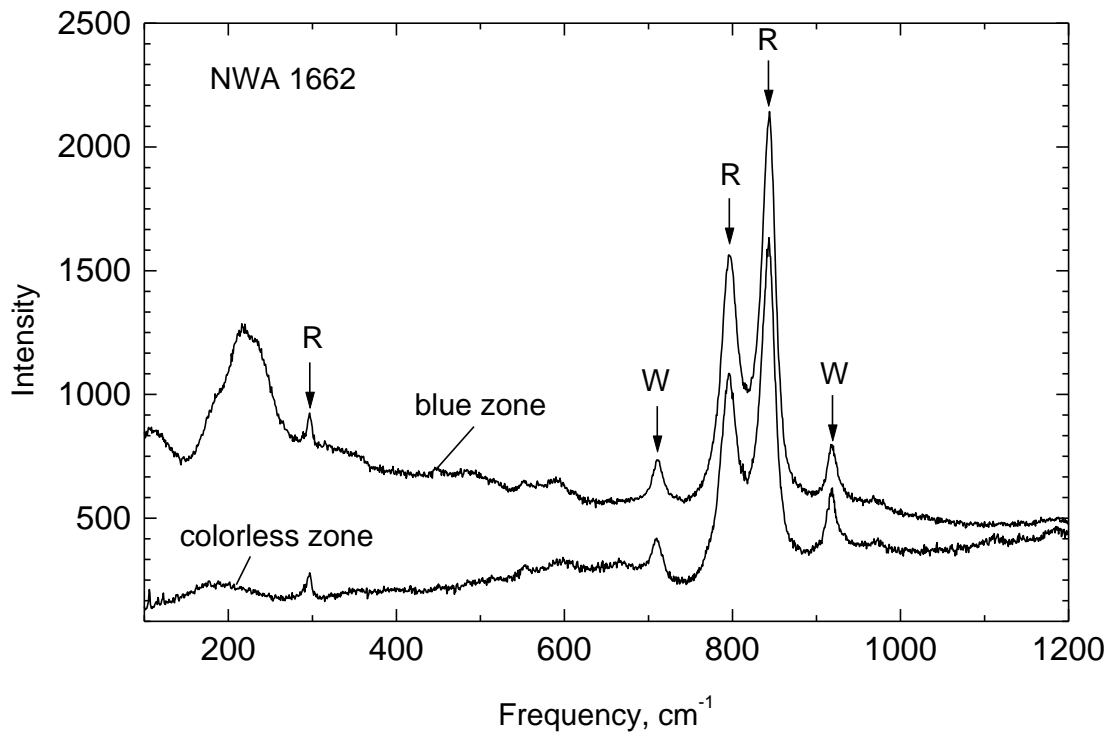


Fig. 1. Raman spectra of blue and colorless zones of a zoned grain (sample #1) of natural ringwoodite in the thin section of the L6 chondrite NWA 1662. R and W denote the lines related to ringwoodite and wadsleyite phase, respectively. The broad structured band at around 225 cm⁻¹ is due to glassy melted phase produced by heating of the laser beam.

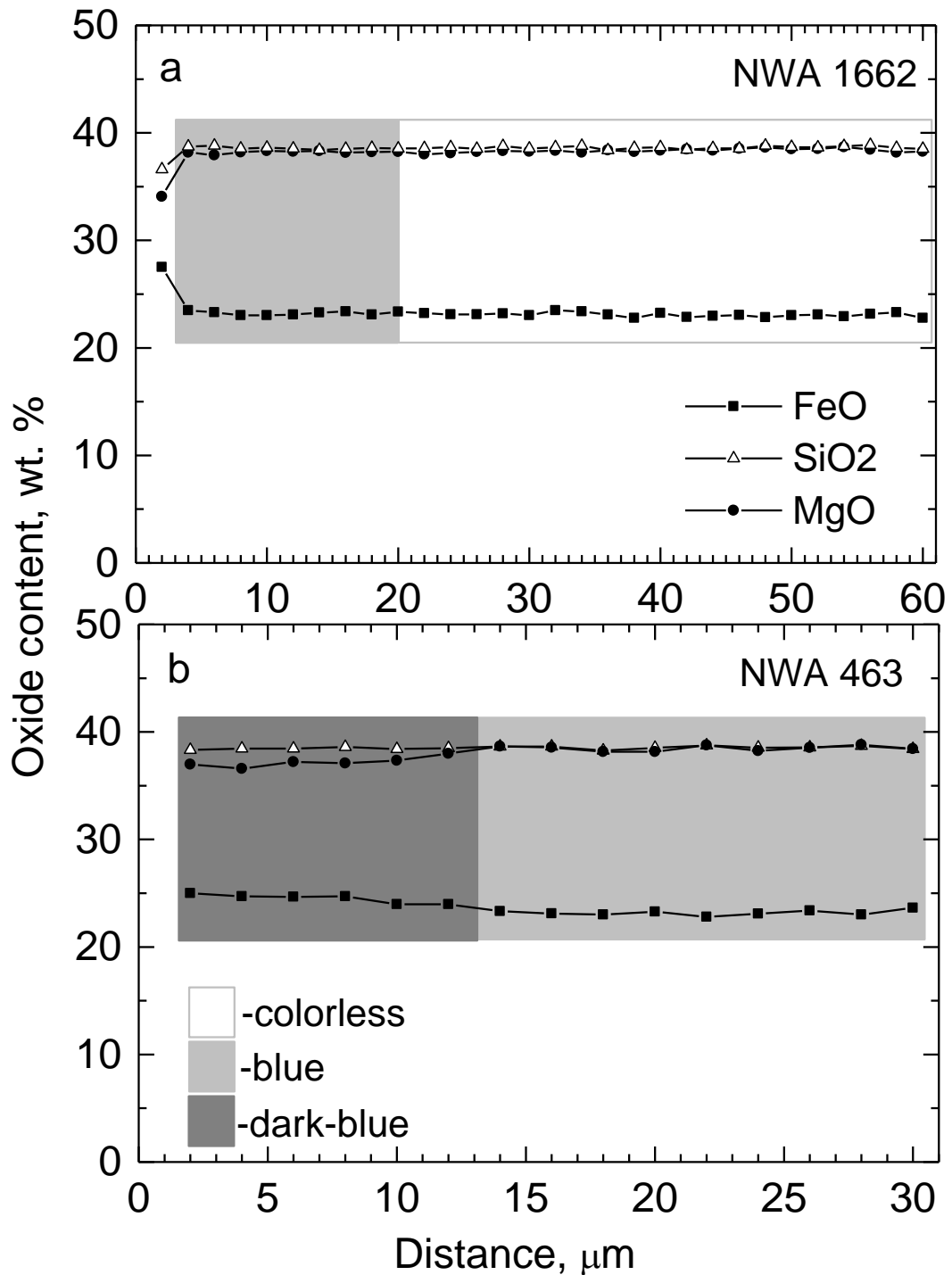


Fig. 2. Profiles of microprobe MgO, FeO and SiO₂ contents traced through differently colored zones of double-colored grain in the thin section of: **a-** NWA 1662 (sample #1) and **b-** NWA 463 (sample #2) L6 chondrites. The first point in **a** is taken very close to the boundary of the grain. Therefore, the data obtained in this point are, most likely, averaged between the ringwoodite grain and the black nontransparent material of the shock metamorphism vein. That why this point drops out of the profiles.

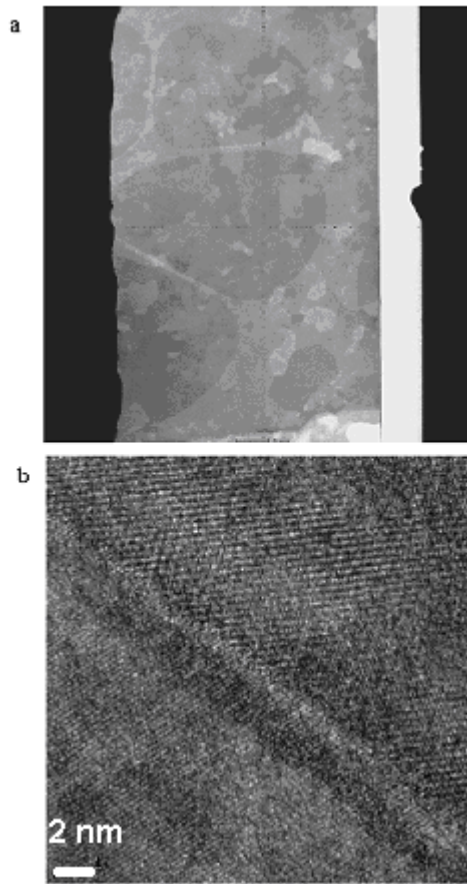


Fig. 3. **a**- HAADF image of a thin foil of natural zoned colorless-dark-blue ringwoodite grain cut over the both zones. No differences between colorless and dark-blue zones are seen. **b**- Image of a boundary between two micrograins of ringwoodite in the dark-blue zone. No evidence of glassy material within the boundary between the grains is seen.

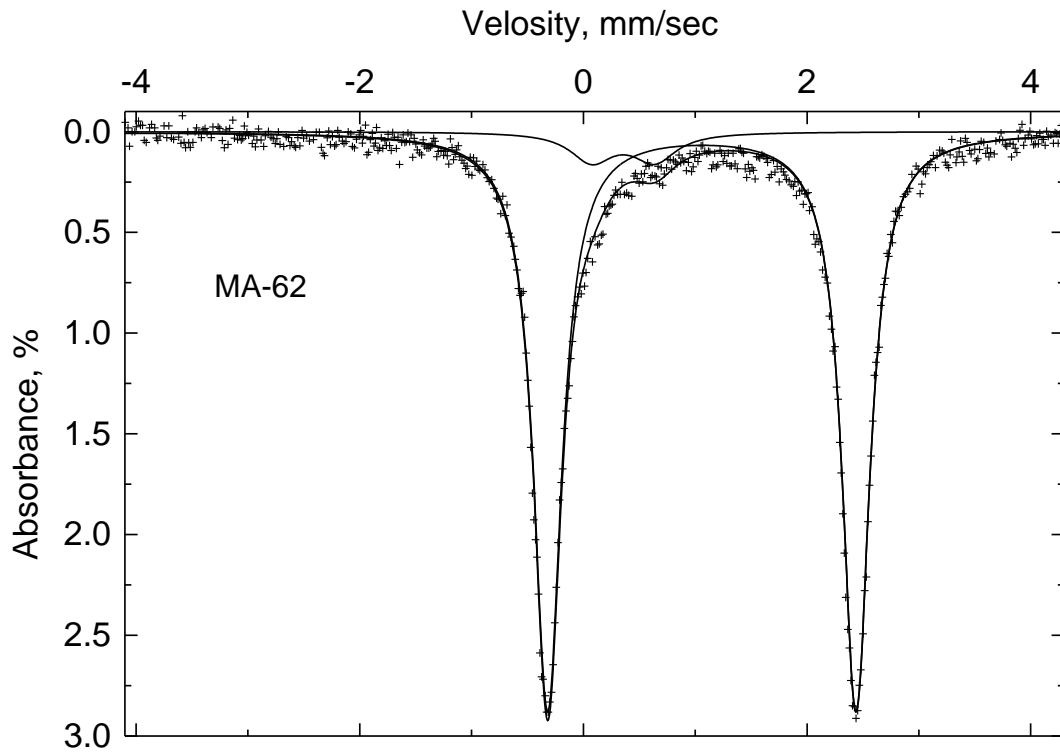


Fig. 4. Mössbauer spectrum of synthetic ringwoodite MA-62 (see Tab. 1). Two quadrupole doublets, the major one with $IS \approx 1.06$ and $QS \approx 2.76$ mm/sec and the junior one with $IS \approx 0.25$ and $QS \approx 0.38$ mm/sec are caused by $^{VI}Fe^{2+}$ and $^{VI}Fe^{3+}$, respectively. The calculated integral intensity ratio of the two QD results to $Fe^{3+}/Fe_{tot} = 0.07$.

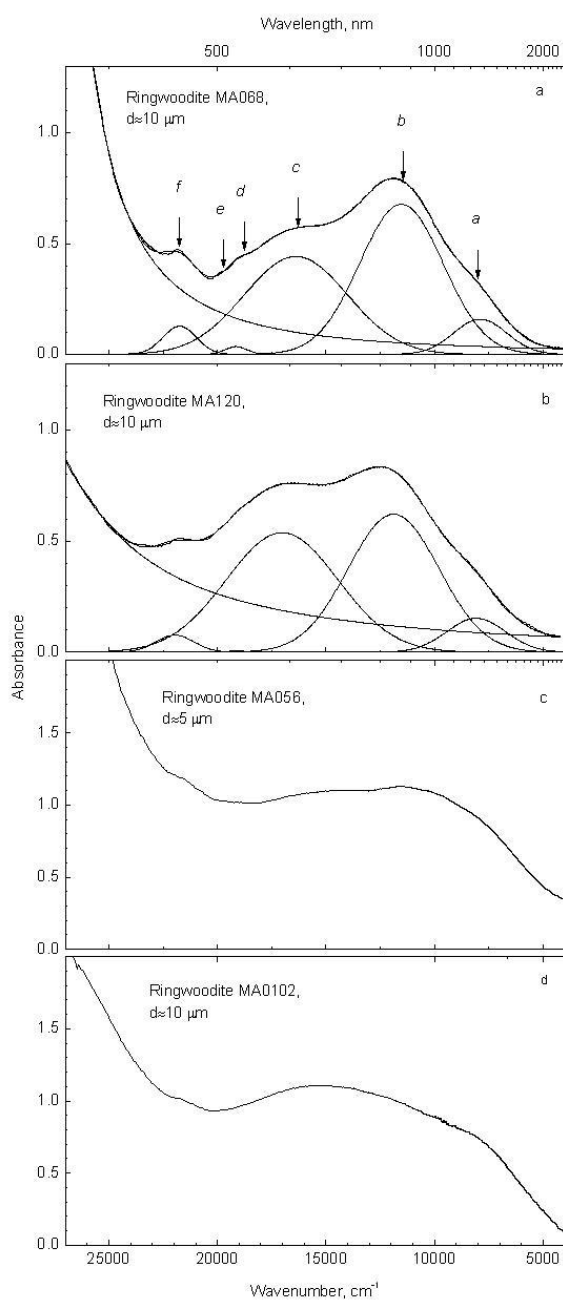


Fig. 5. Optical absorption spectra of thin sections of four synthetic ringwoodite of different composition, MA-68, MA-120, MA-56 and MA-102 (cf. Tab. 1). For MA-68 (a) and MA-120 (b) the result of the curve fitting procedure is also shown. Three broad and intense bands, *a*, *b* and *c*, and three weaker and much narrower bands *d*, *e* and *f*, distinct in the original spectrum, together with the intense high-energy edge, approximated by a sum of a Gaussian and Lorentzian, result to a satisfactory resolution of the spectra. In spectrum of partly oxidized ringwoodite MA-102 (Fig. 5d) predominance of the *c*-band over bands *a* and *b* causes a broad asymmetric absorption envelope with a very smooth maximum at around 15000 cm^{-1} .

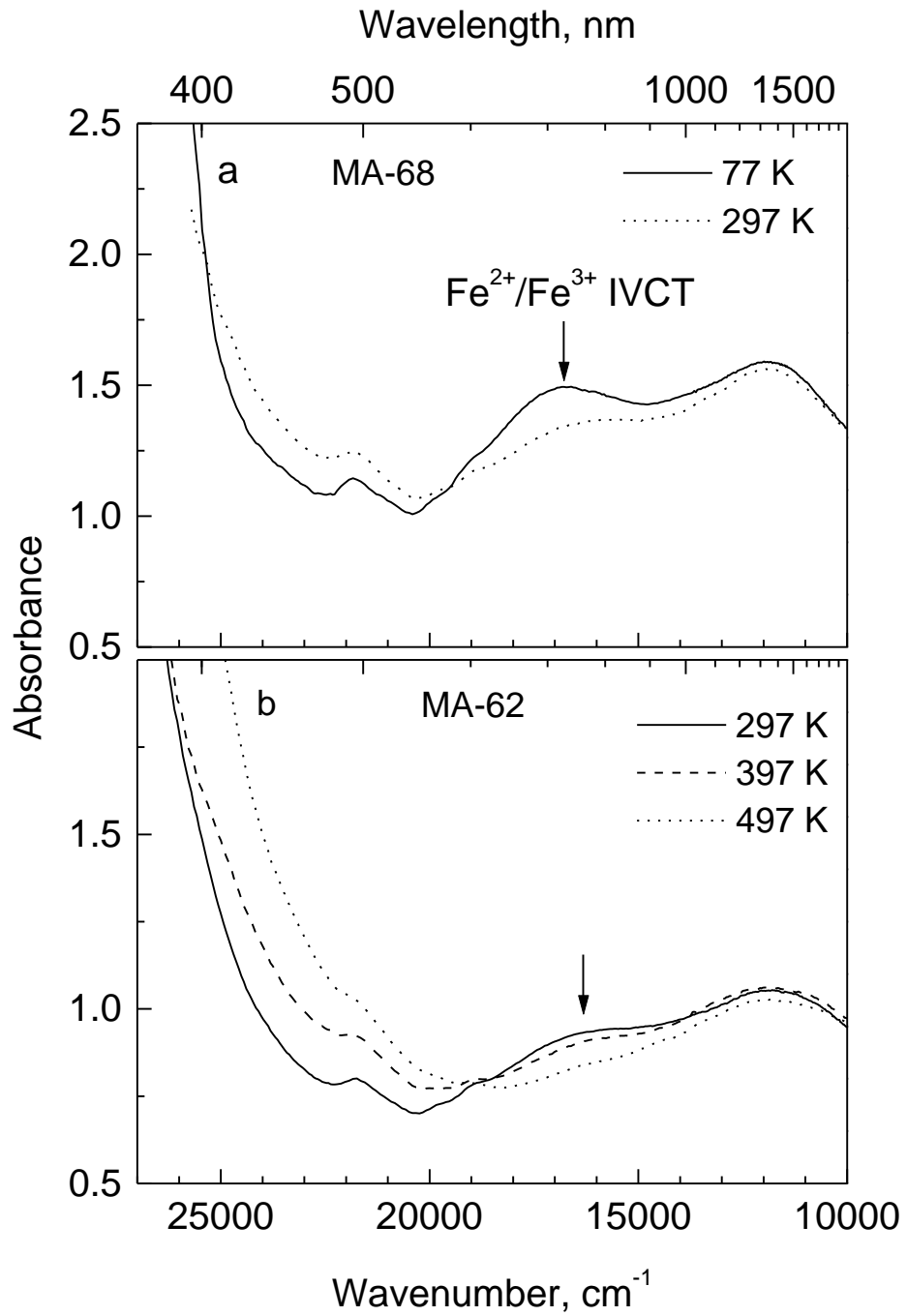


Fig. 6. Absorption spectra of MA-68 (a) and MA-62 ringwoodite (b) measured at different temperatures. Intensity of the *c*-band (denoted at the Figure as Fe²⁺/Fe³⁺ IVCT) displays rather strong temperature dependence different from that of the *b*-band, which practically does not change with temperature.

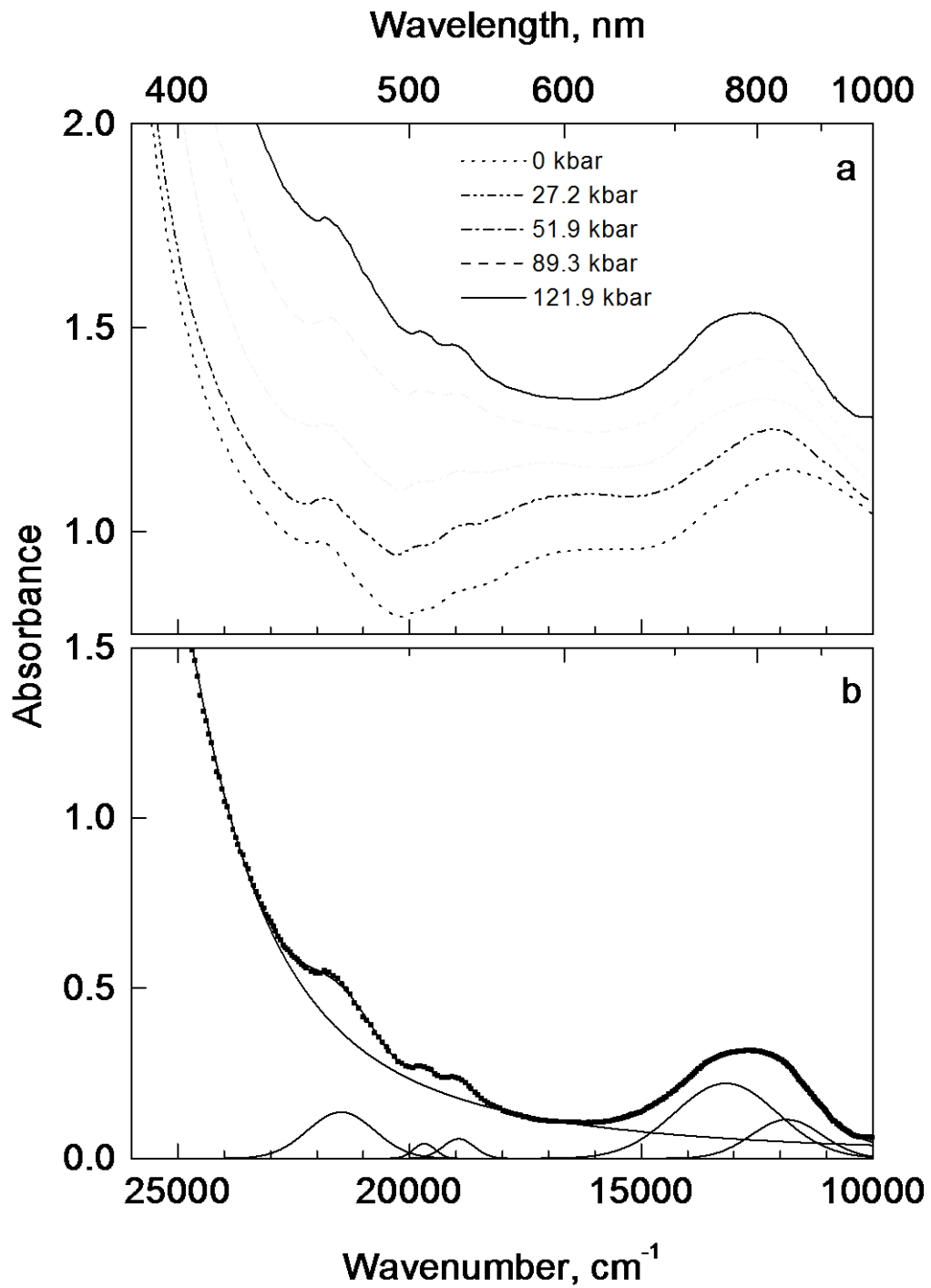


Fig. 7. **a**- Absorption spectra of MA-62 ringwoodite (Tab. 1) measured at different pressures. For the sake of clarity the spectra are shifted along the vertical direction. **b**- The result of the curve fitting procedure of the spectrum measured at 121.9 kbars (ca. 12.2 GPa).

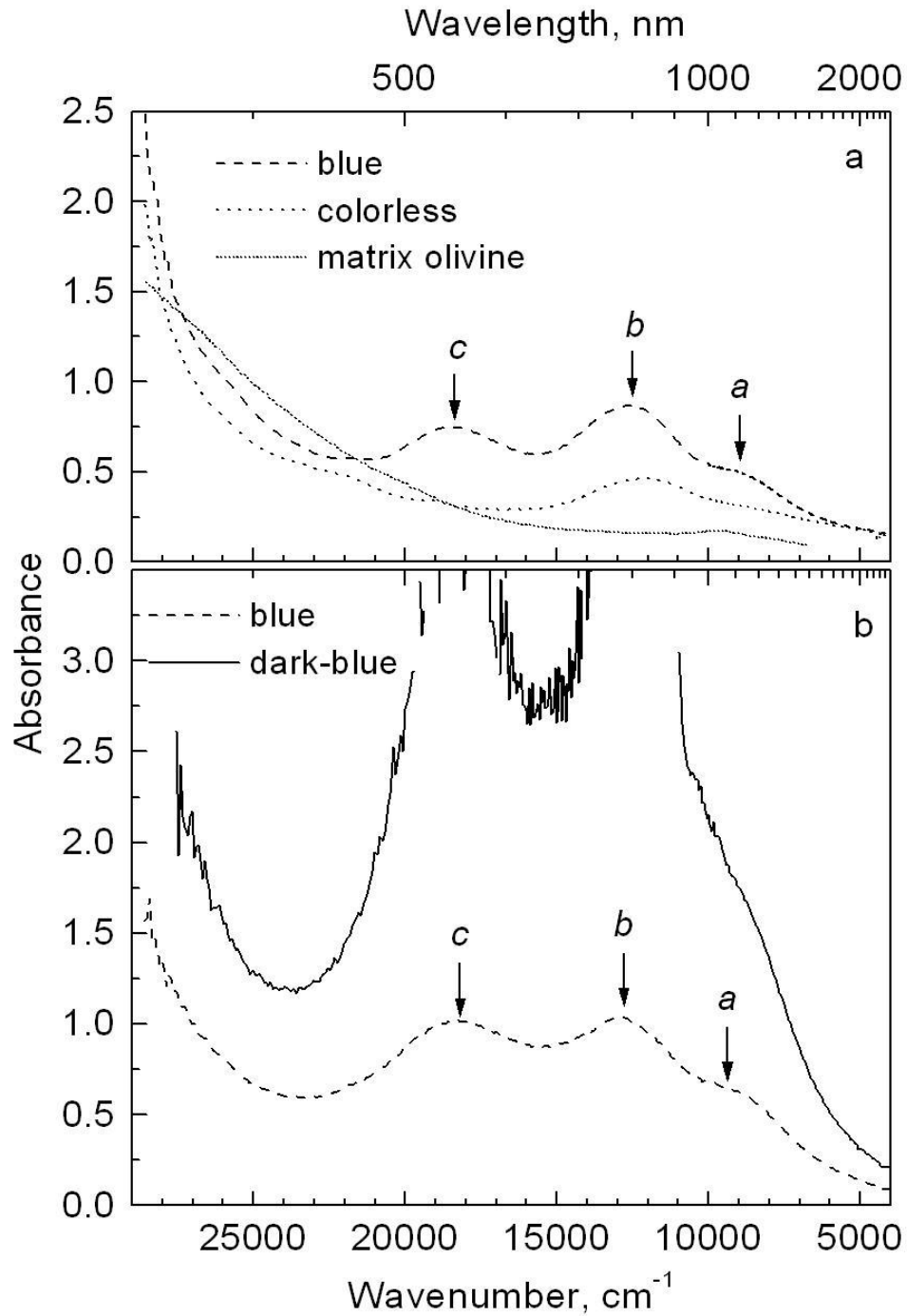


Fig. 8. Optical absorption spectra of differently colored zones in two crystals of natural ringwoodite: **a**- colorless-blue ringwoodite in the thin section of the L6 chondrite NWA 1662 (sample #1). For comparison spectrum of matrix olivine of nearly the same composition as differently colored ringwoodite is also shown; **b**- blue-dark-blue ringwoodite grain in the thin section of the L6 chondrite NWA 463 meteorite (sample #2).

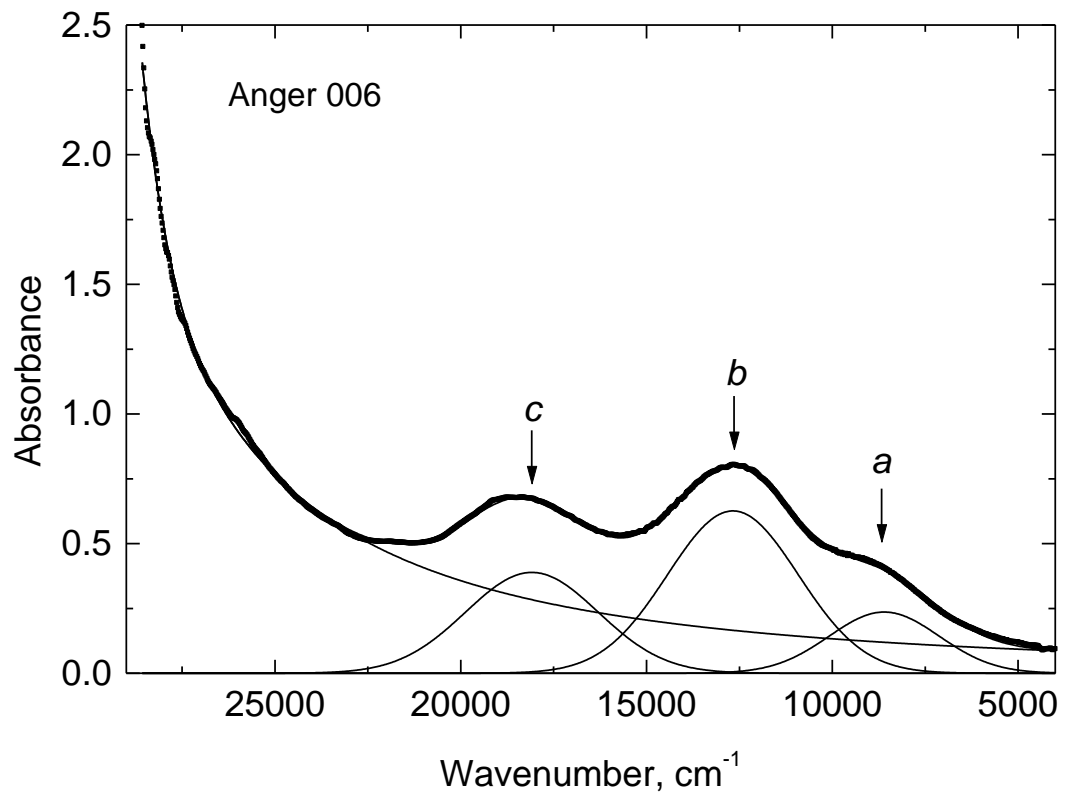


Fig. 9. Result of the curve resolution of the spectrum of blue zone of zoned ringwoodite grain (sample #1) in the thin section of the L6 chondrite NWA 1662 (cf. Fig. 8a).